ZIKV disrupts fetal outcome, placental ultrastructure and drug transporter expression in mice

Short title: ZIKV and placental drug transport

Cherley B. V. Andrade[1], Victoria R. S. Monteiro[1], Sharton V. A. Coelho[2], Hanailly R. Gomes[1], Ronny P. C Sousa[1], Veronica M. O. Nascimento[1], Flavia F. Bloise[1], Stephen G. Matthews[3,4,5,6], Enrrico Bloise[7], Luciana B. Arruda[2], Tania M. Ortiga-Carvalho[1]*.

[1]Institute of Biophysics Carlos Chagas Filho, Federal University of Rio de Janeiro, Rio de Janeiro, RJ, Brazil.

[2] Institute of Microbiology Paulo de Góes, Federal University of Rio de Janeiro, Rio de Janeiro, RJ, Brazil.

[3] Department of Physiology, Faculty of Medicine, University of Toronto, Toronto, Canada.

[4] Department of Obstetrics & Gynecology, Faculty of Medicine, University of Toronto, Toronto, Canada.

[5] Department of Medicine, Faculty of Medicine, University of Toronto, Toronto, Canada.

[6] Lunenfeld-Tanenbaum Research Institute, Mount Sinai Hospital, Toronto, Canada.

[7] Department of Morphology, Federal University of Minas Gerais, Belo Horizonte, BH, Brazil.

Corresponding author: taniaort@biof.ufrj.br (TMO-C)

Competing interests: The authors declare that there are no conflicts of interest.

Abstract

Congenital Zika virus (ZIKV) infection can induce fetal brain abnormalities. Here, we investigated whether maternal ZIKV infection may affect placental physiology and metabolic transport potential, and impact the fetal outcome, regardless of viral presence in the fetus at term. Low (103 PFU-ZIKVPE243; low-ZIKV) and high ($5x10^7$ PFU-ZIKVPE243; high-ZIKV) virus titers were injected into immunocompetent (ICompetent C57BL/6) and immunocompromised (ICompromised A129) mice at gestational day (GD)12.5 for tissue collection at GD18.5 (term). High-ZIKV elicited fetal death rates of 66% and 100%, whereas low-ZIKV induced fetal death rates of 0% and 60% in C57BL/6 and A129 dams, respectively. All surviving fetuses exhibited intrauterine growth restriction (IUGR) and decreased placental efficiency. High-ZIKV infection in C57BL/6 and A129 mice resulted in virus detection in maternal spleens and placenta, but only A129 fetuses presented virus RNA in the brains. Nevertheless, pregnancies of both strains produced fetuses with decreased head sizes ($p<0.05$). Low-ZIKV-A129 dams had higher IL-6 and CXCL1 levels ($p<0.05$) and their placentas showed increased CCL-2 and CXCL-1 contents ($p<0.05$). In contrast, low-ZIKV-C57BL/6 dams had an elevated CCL2 serum level, and increased type I and II IFN expression in the placenta. Notably, increased apoptotic rates, less abundant microvilli and mitochondrial degeneration were evidenced in the placental labyrinth (Lz) of ICompromised and high-ZIKV-ICompetent mice, but not in low-ZIKV-C57BL/6. In addition, decreased placental expression of the drug P-glycoprotein (P-gp), breast cancer resistance protein (BCRP) and the lipid ABCA1 transporters was detected in all ZIKV-infected groups, but BCRP and ABCA-1 were only reduced in ICompromised and high-ZIKV ICompetent mice. Our data indicate that gestational ZIKV infection triggers specific proinflammatory responses and affects placental turnover and transporter expression, in a way dependent on virus concentration and maternal immune status. Placental damage may impair proper fetal-maternal exchange function and fetal growth/survival, likely contributing to congenital Zika syndrome.

Key words: ZIKV, placenta, P-glycoprotein (P-gp) breast cancer resistance protein (BCRP), Abca1, Abcg1, ultrastructure, cytokine, chemokine

Author summary

The ZIKV outbreak in 2016 led to the discovery of several fetal anomalies after viral infection in pregnant women. However, fetal infections were not confirmed in all cases. Thus, virus-induced maternal systemic pathology and/or changes in placental function could be related to fetal Zika congenital syndrome. Therefore, our work aimed to investigate the placental ultrastructure and drug transporter expression in ICompetent and

ICompromised mice and relate these to fetal outcome. We discovered that changes in placental biology, even in ICompetent mice, were associated with impaired fetal development.

Introduction

Congenital Zika virus (ZIKV) infection can be associated with adverse pregnancy outcomes. As such, neonates born from ZIKV-positive pregnancies may develop severe neurological abnormalities, placental pathologies and intrauterine growth restriction (IUGR), among other complications (1). ZIKV vertical transmission has become a major public health issue worldwide, especially in Brazil, where more than 200,000 ZIKV-positive cases have been confirmed, and over 2,000 congenital microcephaly births have been reported (2–6). These numbers represented a 20-fold rise in the incidence of congenital microcephaly in Brazil during the years of the ZIKV pandemic, with similar increases reported elsewhere in Latin America (2,3,7). Importantly, while the ZIKV pandemic is currently thought to be controlled, evidence points to a possible silent ZIKV spread across the Americas (8,9), highlighting the need for improved knowledge of the possible routes of ZIKV vertical transmission and its association with disruptive inflammatory and developmental phenotypes and the need for new avenues of prevention and treatment.

Studies have investigated the possible pathways involved in ZIKV vertical transmission. Miranda and colleagues (10) showed that in humans, ZIKV infection changed the pattern of tight junction proteins, such as claudin-4, in syncytiotrophoblasts. Jurado et al. (2016) suggested that the migratory activities of Hofbauer cells (feto-placental macrophages) could help disseminate ZIKV to the fetal brain (11). Other recent studies have shown that placental villous fibroblasts, cytotrophoblasts, endothelial cells

and Hofbauer cells are permissive to ZIKV, and placentae from ZIKV-infected women had chorionic villi with a higher mean diameter (11–14). However, at present, there is limited information on the precise mechanism of maternal-fetal ZIKV transmission.

Many mouse models have been developed to identify how ZIKV overcomes placental defenses. First, limited information was obtained due to the apparent inability of the virus to infect wild-type (WT) mice (15). ZIKV NS5 targets the interferon signaling pathway in humans but not in mice (16). As such, WT mice develop no clear evidence of clinical disease (16,17) and are of limited use in modeling the disease. However, mice lacking an interferon signaling response show evidence of disease and have been widely used to investigate ZIKV infection during pregnancy (8,16,18).

The interferon system, especially type III interferon, is one of the key mechanisms of host defense and viral targets for immune evasion (19). Type III interferons have a role in protection against ZIKV infection in human syncytiotrophoblasts from term placenta (20). Luo et al. have shown that the inhibition of Toll-like receptors 3 and 8 inhibits the cytokine output of ZIKV-infected trophoblasts (21). In addition, viral replication coincides with the induction of proinflammatory cytokines such as IL-6. This cytokine has a crucial role in inflammation and affects the homeostatic processes related to tissue injury and activation of stress-related responses (22,23). ZIKV infection can trigger an inflammatory response with IL-6 release (11,24).

Maternal infection has profound effects on placental permeability to drugs and environmental toxins. Changes in the expression and function of specific ABC transporters in the placenta and yolk sac following infective and inflammatory stimuli have been demonstrated (25–29). ABC transporters are efflux transporters that control the biodistribution of several endogenous and exogenous substrates, including xenobiotics (antiretrovirals, synthetic glucocorticoids), steroid hormones (estrogens,

androgens), nutrients (folate, cholesterol) and immunological factors (chemokines and cytokines) within the maternal-fetal interface (30). The best described ABC transporters in the placenta are the multidrug resistance P-glycoprotein (P-gp), the breast cancer resistance protein (Bcrp) and the lipid Abca1 and Abcg1 transporters. P-gp and BCRP transporters are responsible for preventing fetal accumulation of xenobiotics and environmental toxins that may be present in the maternal circulation, whereas ABCA1 and ABCG1 control the placental exchange of cytotoxic oxysterol and lipid permeability throughout pregnancy; therefore, they play an important role in fetal protection and placental lipid homeostasis (25).

Despite a limited number of studies showing ZIKV infection in immunocompetent mice, it was previously demonstrated that intrauterine inoculation of high virus titer resulted in decreased fetal viability, with worse outcomes following infection in early gestation (31). In another report, intravenous infection at very early embryonic day resulted in fetal demise even though the virus was not found in the fetal compartment in most treated animals (32). In the present study, we hypothesize that maternal exposure to ZIKV affects placental function, including placental ultrastructure and ABC transporter (P-gp, Bcrp, Abca1 and Abcg1) protein expression, even in the absence of vertical transmission and that these effects are dependent on viral infective titers and maternal immune status.

Results

Weight gain across pregnancy is dependent on maternal immune status in ZIKV-infected mice.

To determine the effect of ZIKV infection on fetal and placental phenotypes at term (GD18.5), we infected ICompetent C57BL/6 and immunocompromised (ICompromised) A129 mice with ZIKV at GD12.5 (Fig 1A). Given the very distinct susceptibility of C57BL/6 and A129 mice to ZIKV, systemic infection models were established by injecting high ($5x10^7$ PFU) and low (10^3 PFU) virus inoculum titers. As shown in Table 1, ICompetent C57BL/6 mice from all groups and ICompromised A129 dams inoculated with mock and low ZIKV exhibited higher maternal weight at GD18.5 than at GD12.5 and GD0.5 ($p<0.05$). On the other hand, ICompromised A129 mice presented significant weight loss at GD18.5, despite showing an increase at GD12.5 in relation to GD0.5.

Table 1: Maternal weight gain throughout pregnancy

	ICompetent			ICompromised		
Maternal weight (g)	**Mock (n=11)**	**High (n=15)**	**Low (n=9)**	**Mock (n=3)**	**High (n=3)**	**Low (n=3)**
GD0.5	22.4±0.7[a]	23.0±0.6[a]	21.9±0.7[a]	21.7±1.9[a]	21.7±0.9[a,b]	25.0±1.0[a]
GD12.5	25.5±0.6[b]	26.2±0.8[b]	25.1±0.5[b]	25.3±1.2[a]	26.0±1.0[a]	28.0±0.6[a]
GD18.5	31.6±0.7[c]	30.3±0.9[c]	31.4±1.1[c]	32.0±1.5[b]	20.0±1.5[b]	30.7±0.3[b]
ΔGD12.5-0.5 (Δ)	4	3	3	3	4	3
ΔGD18.5-0.5 (Δ)	9	7	10	10	-2	5

GD=gestational day; Δ=delta; values are expressed as the mean±standard error of the mean (SEM). One-way ANOVA followed by Tukey's test analyzed differences among GD0.5, 12.5 and 18.5 in each group; different letters indicate $p<0.05$.

Immunocompetent and immunodeficient mice have distinct term placental and fetal phenotypes in response to high and low ZIKV titer challenges in mid-pregnancy.

The fetuses from C57BL/6 dams and sires were called ICompetent. The fetuses from the mates of A129 dams and C57BL/6 sires were called ICompromised. High-ZIKV ICompetent mice exhibited 34% fetal loss, whereas high-ZIKV-A129 mice had 100% fetal loss (Fig 1B). In the low-ZIKV groups, C57BL/6 mice had no (0%) fetal death, while A129 mice exhibited a 42% fetal death rate (Fig 1B). Fetal and fetal head sizes were decreased in A129 mice compared to those in C57BL/6 dams infected with the high ZIKV titer (p=0.05; Fig 1 C-F). However, no changes in fetal weight and fetal head sizes were observed when the mice were infected with the lower ZIKV titer (Fig 1 C-F).

ZIKV is detected in the fetal brain of ICompromised, but not ICompetent mice.

ZIKV RNA was detected in the spleens of pregnant ICompetent C57BL/6 mice inoculated with the highest ZIKV titer, confirming acute systemic infection. Viral RNA was also detected in the majority of placentae of those mice (Fig 2A-B) but not in the maternal and fetal C57BL/6 brains (Fig 2A-B), suggesting that the virus was not transmitted to the fetuses. Although low ZIKV inoculation resulted in virus detection in the spleens of pregnant C57BL/6 mice, infection was not evidenced in the placentae or fetal brains. In contrast, ZIKV RNA was detected in all analyzed organs from ICompromised A129 dams, including the maternal brain and spleen and the placenta and fetal brain (Fig 2A-B). Viremia in maternal serum was evaluated at 4, 48 and 144 hours after infection. Within 4 hours, the presence of the virus was verified in the serum (high ICompetent = 637.5 PFU/mL, low ICompetent = 740 PFU/mL and low ICompromised = 325 PFU/mL), indicating that the virus was correctly inoculated. Afterwards, ZIKV RNA was detected in ICompromised dams at 48 and 144 hours postinoculation but not in ICompetent dams.

ZIKV infection induces distinct systemic and placental inflammatory responses in ICompetent and ICompromised mice.

The maternal serum and placental protein levels of specific cytokines and chemokines related to fetal death and preterm delivery (33–35) were evaluated to probe whether midgestation ZIKV infection would induce a maternal inflammatory response at term in our two distinct models. Since A129 infected with 10^7 ZIKV-PFU showed 100% fetal loss, we proceeded using 10^7 PFU inoculation in C57BL/6 and 10^3 PFU inoculation in both C57BL/6 and A129 mice.

CCL2 was elevated in the serum of low-ZIKV ICompetent mice, but no other alteration was systemically detected in any ICompetent mice at this time point (Fig 3A-B). On the other hand, ICompromised dams showed significantly increased CXCL1 and IL-6 levels in the serum, and a strong trend for an enhancement in CCL2 (Fig 3C). Analysis of cytokines and chemokines expression at the placenta demonstrated that CXCL1 and CCL2 chemokines were also upregulated in the ICompromised, but not of ICompetent mice (Fig 3 D-F). Surprisingly, IL-6 protein expression was augmented in some of the low-ZIKV ICompetent mice (58%; $p<0.05$), but not in high-ZIKV nor ICompromised mice (Fig 3D-F).

We also assessed the placental mRNA expression of a range of cytokines related to placental infective responses: Ifn-γ, Il-6, Ifn-1, Tnf-α, Il-1β, and Il-10. All the infected mice showed a significantly increase in TNF-a mRNA expression, with higher levels detected in ICompetent mice (Fig 3G-I). The low-ZIKV ICompetent mice presented a modest, but significant type I IFN expression, which was not detected in the high-

ZIKVgroup (Fig 3G). Additionally, both low-ZIKV infected groups (ICompetent and ICompromised) presented increased Ifn-γ mRNA expression (Fig 3G and 3I, $p< 0.05$). Interestingly, placental Il-6 mRNA levels were only elevated in ICompromised pregnancies compared to the mock ($p=0.05$) (Fig 3I). Il-1b and IL-10 remained unchanged in all groups analyzed (Fig 3 G-I).

ZIKV affects placental proliferation, apoptosis and ultrastructure in a viral load- and maternal immune status-dependent manner.

We did not observe changes in placental weight or in the fetal:placental weight ratio in any of the groups investigated (data not shown). However, since we detected the presence of ZIKV RNA in the placentas, we investigated the cellular proliferation (Ki-67^+ cells) and apoptotic ratio in the labyrinth zone (Lz) and junctional zone (Jz) of the mouse placenta. Increased Ki-67 staining was observed in the Lz of high- and low-ZIKV-treated ICompetent animals compared to mock animals (Fig 4A, $p=0.005$ and $p=0.015$), whereas the Lz apoptotic ratio was increased in high- and decreased in low-ZIKV dams ($p=0.01$, Fig 4B). A similar apoptotic pattern was detected in the Jz of ICompetent pregnancies ($p=0.008$ and $p=0.004$, respectively; Fig 5B), although no differences were observed in Ki67 staining (Fig 5A). In contrast, in ICompromised dams, Lz Ki-67 staining was decreased ($p=0.001$; Fig 4C), while the apoptotic reaction was increased in ZIKV-infected animals ($p=0.05$; Fig 5D). Jz from ICompromised offspring exhibited increased Ki-67 labeling and no differences in the apoptotic reaction ($p=0.001$; Fig 5 C-D).

Placental ultrastructure is differently impacted by high- and low-titer ZIKV infection in ICompetent and ICompromised strains.

Ultrastructural analyses in the Lz of ICompetent and ICompromised-mock animals detected sinusoidal trophoblastic giant cells exhibiting regular microvilli, euchromatic nuclei, preserved mitochondrial ultrastructure and regular narrow ER cisternae (Fig 6A and 6D). In sharp contrast, high-ZIKV ICompetent (Fig 6B) and low-ZIKV ICompromised infected placentae (Fig 6E) showed fewer villi in the sinusoidal giant trophoblastic cells, degenerated mitochondria, granular ER with dilated cisterns and euchromatic nuclei. The sinusoidal giant trophoblastic cells from the low-ZIKV ICompetent (Fig 6C) also had fewer villi and degenerated mitochondria than the mock placentae, but there and had no effect on the ER or euchromatic nuclei.

The Jz of mock ICompetent and ICompromised (Fig 7A and 7 D) and of low-ZIKV ICompetent (Fig 7C) placentae exhibited euchromatic nuclei, with evident heterochromatin, preserved mitochondria and narrow cisternae granular ER. High-ZIKV ICompromised and low-ZIKV ICompromised placentae had degenerated mitochondria, granular ER with dilated cisterns and euchromatic nuclei (Fig 7B and 7 -E).

ZIKV differentially affects placental expression of drug and lipid ABC transporter systems.

Evaluation of key ABC transporters in the Lz of mock and ZIKV-infected ICompetent and ICompromised placentae revealed that immunolabeling of the drug P-gp and Bcrp efflux transporter systems was primarily present at the cellular membranes of the sinusoidal trophoblastic giant cells, with diffuse cytoplasmic Bcrp staining. Labeling of the Abca1 and Abcg1 lipid efflux transporters was moderately and heterogeneously distributed within the Lz. Less Lz-P-gp was observed i n ICompetent mice infected with both high- and low-ZIKV infective regimens, in comparison to mock-treated animals (p=0.001 and p=0.002, respectively; Figure 8A), whereas Bcrp and Abca1 staining was only reduced was observed in high-ZIKV-infected mice (p=0.003 and p=0.004, respectively; Figure 8B-C). P-gp, Bcrp and Abca1 transporter immunostaining was downregulated in ICompromised low ZIKV-treated animals (p=0.001, p=0.05 and p=0.05, respectively; Figure 9A-C). No changes in Abcg1 were observed in any of the experimental groups (Figure 8D and Figure 9D).

Next, the impact of ZIKV on ABC transporters in the Jz layer (structural and endocrine layers of the mouse placenta) was assessed. P-gp and Bcrp were predominantly localized at the cellular membranes of spongiotrophoblast cells, whereas Abca1 and Abcg1 exhibited membrane and cytoplasmic staining. P-gp staining was decreased in Jz cells from the low-ZIKV ICompromised placentae (p=0.006), with no other alterations observed (Fig 10A-D and Fig 11A-D).

Discussion

In this study, we investigated several fetuses and placentas features at term (GD18.5) in ICompetent (C57BL/6) and ICompromised (A129) mice exposed to ZIKV at mid-pregnancy (GD12.5). Fetal survival rates, systemic and placental inflammatory responses, placental ultrastructure and cell turnover, as well as the expression of key drug (P-gp and Bcrp) and lipid (Abca1) efflux transporter systems in the placenta, were consistently impacted by ZIKV in both strains. The magnitude of the effects was is clearly related to the infective titer (high and low) of ZIKV and maternal immune status (ICompetent-C57BL/6 x and ICompromised-A129) and fetal alterations were not exclusively dependent on the virus detection in the fetuses.

Infection of ICompetent mice with ZIKV did not result in viremia in the initial postinoculation phase, although viral RNA was detected in the maternal spleen in both the high- and low-ZIKV groups, confirming systemic infection. This is consistent with a previous report (36). Our data demonstrate that pregnant ICompetent C57BL/6 mice

were more susceptible to higher ZIKV than to lower ZIKV infective titers. Since viral RNA was only detected in the placentae of high ZIKV, and fetal survival rates and weight were impacted to a greater extent in those mice. Strikingly, even though the virus was not present in the fetal brain (at least at term), fetal and fetal head weights were lower in the high-ZIKV titer regimen, suggesting that high infective viral load in mid-pregnancy, even in ICompetent individuals, can induce IUGR and lower fetal head weight despite a lack of transmission to the fetal brain (37). On the other hand, ICompromised placentae and fetal brains had detectable viral transcripts, with no changes in weight, which is consistent with previous data (18). In fact, in our models, the presence (ICompromised) or the absence (ICompetent) of the virus in the fetal brain did not correspond to fetal head size (decreased in only high ICompetent). The data from ICompetent and ICompromised placentae demonstrate how important the maternal immunological status is to control viremia, fetal survival and accessibility of the virus into the fetal brain. The reason for the reduction in fetal brain size in C57BL/6 mice in the absence of fetal brain infection requires further investigation. It is possible that fetal brains of the ICompetent mice may have been exposed to ZIKV earlier in pregnancy when viremia was present in the maternal blood, and this may have severely compromised brain development.

A distinct inflammatory profile was also detected in the three analyzed groups. At the protein level, low-ZIKV-ICompromised dams exhibited increased maternal IL-6 and CXCL-1 and placental CCL-2 and CXCL-1, whereas low-ZIKV-ICompetent dams had increased maternal CCL2 and placental IL-6 levels. CCL-2 and CXCL-1 are related to fetal death and preterm delivery (33–35), and could be associated with pronounced fetal injure detected upon ICompromised pregnancy. In addition, it was previously demonstrated (38) that IL-6 is related to fetal response syndrome, characterized

by activation of the fetal immune system. This syndrome is known to increase fetal morbidity and affect several organs, such as the adrenal gland, brain and heart (31,38–41). At the mRNA level, IL6 expression was only detected in ICompromised placentae at term and may indicate a sustained harmful response in these mice until term. IFN signaling pathway may be triggered by ZIKV (16) and represents one of the key mechanisms of host defense and viral targets for immune evasion (19), but we did only detected a slight increase in type I IFN in low-ZIKV ICompentent mice at term. However, we cannot rule out the possibility that these cytokines might have been produced earlier. IFN-g expression was significantly enhanced in both ICompetent and ICompromised low-ZIKV derived placentas, but not in the high-ZIKV infected mice. Although we could not assess cytokine expression in high-ZIKV ICompromised placentas, one may extrapolate that low-ZIKV infection could result in stimulation of IFN-g-producing cells, which has been previously showed to be protective for ZIKV-infected mice (Lucas, et al., 2018).

Both ICompromised and ICompetent mice showed increased expression of of placental *Tnf-α* mRNA, which has been demonstrated to be is directly related to placental damage, abortion and premature birth (REF). In addition increased TNF-a response is relatated to impaired placental hormone production and trophoblastic invasion and increasedapoptosis in pregnancy (42,43). Although we did not assessed TNF-a protein levels in the placenta and maternal blood, this response could be implicated in the overall damage detected.

Although differences in placental weight were not observed, ZIKV infection mid-pregnancy had a profound effect on placental cellular turnover, dependent on titer, strain and/or placental compartment. Lz is responsible for fetal and maternal nutrient, gas and

waste exchange, while Jz provides structural support, nutrient storage and hormone synthesis (49). ZIKV induced a consistent increase in Lz proliferation in all groups. However, the Lz apoptotic rate was increased only in the high-ZIKV-ICompetent and ICompromised groups and decreased in low-ZIKV-ICompetent mice. The mechanisms underlying these differences are unknown but may be related to the distinct maternal and placental proinflammatory responses and/or to the direct effect of the virus on the placenta (50). Increased Lz apoptosis in the high-ICompetent-ZIKV group may be one of the mechanisms driving the lower fetal and fetal head weight detected in this group. In this context, changes in placental turnover can determine placental maturation and function and lead to fetal distress and developmental abnormalities (51). An increase in the Lz apoptotic ratio may signify damage to this placental layer, which is consistent with the fact that diverse pathological lesions associated with congenital disorders were described in placentae from women infected by ZIKV at different stages of pregnancy (52). Conversely, no proliferative changes were observed in Jz in high-ZIKV and low-ZIKV ICompetent mice, while increased and decreased apoptotic rates were detected. It follows that the lack of Jz-Ki-67 induction may suggest that this layer is less capable of restoring proliferation in response to high-ZIKV challenge, and this may be related to decreased fetal growth.

Our placental ultrastructural analysis detected consistent differences across ZIKV-exposed groups. The Lz and Jz layers from both strains exhibited signs of ER stress, i.e., dilated ER cisterns or fragmented ER granular structures. These alterations may result from the accumulation of folded or poorly folded viral proteins in the ER lumen (53–55). It has been demonstrated that the *Flaviridae* family uses the ER to replicate (56), and according to Offerdahl et al. (2017)(53), there is evidence of ZIKV interacting with this organelle, promoting an increased release of Ca^{+2} from the ER to the

cell cytoplasm, thereby causing an increase in the production of reactive oxygen species (ROS) (57,58).

The mitochondrial ultrastructure in the Lz and Jz layers was severely impacted by ZIKV exposure. We found evidence of mitochondrial degeneration, i.e., mitochondrial membrane rupture, absence of mitochondrial ridges and less electron-dense mitochondrial matrix in all treated groups. Placental mitochondrial dysfunction is associated with IUGR (59,60) and may be related, at least in part, to the lower fetal weight observed in high-ZIKV-ICompetent fetuses along with the altered placental apoptotic and proliferative patterns. Furthermore, mitochondrial dysfunction together with ER stress is likely to modify the placental ROS balance and generate local oxidative stress (61), which is associated with impaired fetal development (62). Of importance, associations between mitochondrial disruption, ER stress and placental cell senescence have been reported. Senescence is characterized as an ir reversible interruption of the cell cycle and acquisition of a senescence-associated secretory phenotype (SASP) that promotes the release of cytokines such as Il-1, Il-6, Il-8 and proinflammatory proteases (62). Therefore, the increased expression of IL-6 detected in the placentas of ICompromised mice suggest a SASP profile, which may be related to changes in the ER and mitochondrial ultrastructure, accompanied by important changes in apoptosis and cell proliferation . The interactions between mitochondria and the ER are critical for homeostasis and cell signaling (63). In conjunction with the ER, mitochondria can regulate cell death mediators in response to hypoxia and inflammation (64). The increase in apoptosis observed in the high-titer ICompetent groups and the low-titer ICompromised group may be related to the mitochondrial damage and ER stress observed. In fact, we observed an important decrease in microvillus abundance in sinusoidal giant trophoblast cells. Previously, we observed a decrease in microvillus density in the Lz of pregnancies exposed to malaria in

pregnancy (MiP) (65). Together, our data show that different gestational infective stimuli (MiP and ZIKV) are capable of damaging placental microvillus abundance and impairing proper fetal-maternal exchange function and fetal growth/survival.

Next, to investigate whether maternal ZIKV exposure may influence fetal protection, we evaluated the placental localization and expression (semiquantitative) of the ABC efflux transporter systems P-gp, Bcrp, Abca1 and Abcg1, which are highly enriched in labyrinthine microvilli and in human syncytiotrophoblasts. These efflux transporters exchange drugs, environmental toxins, cytotoxic oxysterols and lipids within the maternal-fetal interface (25). We found a consistent decrease in labyrinthine P-gp expression in all ZIKV-exposed groups, demonstrating that ZIKV infection during pregnancy has the potential to increase fetal exposure to P-gp substrates such as synthetic glucocorticoids, antibiotics, antiretrovirals, antifungals, stomach-protective drugs, and nonsteroidal anti-inflammatory drugs (25). Furthermore, Jz-P-gp was decreased in ICompromised placentae. Although little is known about the Jz function of ABC transporters, our data highlight the need for further studies investigating the biological importance of ABC transporters in the placental endocrine and structural zones of the rodent hemochorial placenta under normal and infective conditions.

ZIKV impaired Lz Bcrp and Abca1 expression in ICompetent (high) and ICompromised (low) mice. However, no effects were observed in ICompetent animals at a low ZIKV titer or in Abcg1 in any experimental setting. As such, ZIKV also likely increases the fetal accumulation of Bcrp substrates (antibiotics, antiretrovirals, sulfonylureas, folate, mercuric species, estrogenic mycotoxins, carcinogens phototoxic compounds, among others) and disrupts placental lipid homeostasis (lipids, cholesterol, cytotoxic oxysterols) by reducing placental Abca1 expression (25,66–69). We can

speculate that the increased fetal accumulation of the P-gp, Bcrp and Abca1 substrates during ZIKV infection may contribute to the establishment of congenital Zika syndrome, although additional studies are clearly required to answer this important question. The current data are in agreement with previous publications showing that bacterial, viral and protozoan inflammation alters the expression and/or function of P-gp, Bcrp and Abca1 in biological barriers such as the placenta, yolk sac and blood-brain barriers (25,27,56,65,70–72).

Conclusion

Our data show that gestational ZIKV impacts the fetal phenotype independently of term fetal viremia. Abnormal placental cell turnover, ultrastructure and transporter expression may result from the specific proinflammatory responses that depend on the ZIKV infective load and maternal immune status. Fetal accumulation of drugs, environmental toxins and lipids within the fetal compartment may be potentially increased in ZIKV-infected pregnancies due to altered levels of key ABC transporters.

Materials and methods

Virus preparation and storage

The Brazilian $ZIKV_{PE243}$ (GenBank ref. number KX197192) strain was isolated from a febrile case during the ZIKV outbreak in the state of Pernambuco, Brazil and was kindly provided by Dr Ernesto T. Marques Jr. (Centro de Pesquisa Aggeu Magalhães, FIOCRUZ, PE). Viruses were propagated in C6/36 cells with viral titers determined by

plaque assays in Vero cells, as previously described (73). Supernatants of noninfected C6/36 cells cultured under the same conditions were used as mock controls.

Animal experimentation and study design

Two mouse strains were used in the study: ICompetent C57BL/6 and ICompromised (type 1 *Ifnr*-deficient) A129 strains. Since we were unable to consistently produce viable pregnancies by mating A129 males and females in our experimental settings, we mated A129 females (n=15) with C57BL/6 males (n=4) to produce ICompromised C57BL6/A129 pregnancies, whereas ICompetent C57BL/6 pregnancies were obtained by mating male (n=6) and female (n=35) C57BL/6 mice (8-10 weeks old). Animals were kept in a controlled temperature room (23°C) with a light/dark cycle of 12 hours and *ad libitum* access to water and food. After detecting the proestrous/estrous phase by vaginal cytology, copulation was confirmed by visualization of the vaginal plug and considered gestational day 0.5 (GD0.5). Maternal weight was monitored for confirmation of pregnancy; thus, females were weighed on GD0.5 and GD12.5, and females with a weight gain greater than 3 g were considered pregnant and entered randomly in the experimental groups. Experimental protocols were approved by the Animal Care Committee of the Health Sciences Center, Federal University of Rio de Janeiro (CEUA-036/16 and 104/16) and registered within the Brazilian National Council for Animal Experimentation Control.

On GD12.5, pregnant mice (ICompetent and ICompromised pregnancies) were injected with a single intravenous (i.v.) titer of ZIKV or mock control. ICompetent and ICompromised pregnant mice were randomly subdivided into three experimental groups: the mock (control) group, which received supernatants of noninfected C6/36 cell injection (ICompetent mock and ICompromised mock); the high-ZIKV-titer group, inoculated

with $5x10^7$ plaque-forming units (PFU) of $ZIKV_{PE243}$ (ICompetent high and ICompromised high); and the ZIKV low-titer group, injected with 10^3 PFU of $ZIKV_{PE243}$ (ICompetent low and ICompromised low).

On the morning of GD18.5, all animals were euthanized with a sodium phenobarbital overdose of 300 mg/kg. Maternal blood was collected by cardiac puncture, centrifuged (10 min, 4000 g) and stored at -20°C. The maternal brain and spleen, all placentae and all fetuses were dissected, collected and weighed, followed by fetal head isolation and measurement. The three placentae closest to the mean weight in a litter were selected for further analysis and cut in half using umbilical cord insertion as a reference (49,65,74). One-half of the placental disk was frozen in liquid nitrogen for qPCR, and the other half was fixed overnight in buffered paraformaldehyde (4%, Sigma-Aldrich, Brazil) for ultrastructural and protein expression/localization analysis. Matched fetal heads, maternal brains and spleens were frozen in liquid nitrogen for qPCR.

ZIKV RNA quantification by qPCR

ZIKV load was evaluated in maternal blood, brains and spleens and in the placentae and fetal heads. Brains, spleens, placentae and fetal heads were macerated in RPMI medium (Gibco™ RPMI 1640 Medium) normalized by the ratio of 0.2 mg of tissue to every 1 µl of medium and plotted per gram of tissue. The macerated volume was centrifuged at 4500 g for 5 min to remove tissue residues, and then 500 µl of the centrifuged volume was used for RNA extraction using 1 mL of TRIzol reagent (Life Technologies, Thermo Fischer, USA). Treatment with DNase I (Ambion, Thermo Fischer, USA) was performed to prevent contamination by genomic DNA. cDNA was synthesized using a cDNA High Capacity Kit (Applied Biosystems, Thermo Fischer, USA) according to the manufacturer's instructions by subjecting the samples to the

following cycle: 25°C for 10 min, 37°C for 120 min and 85°C for 5 min. qPCR was performed using a StepOnePlus Real-Time PCR system and TaqMan Master Mix Reagents (Applied Biosystems, Thermo Fischer, USA) using primers and probes specific for the protein E sequence (75). Samples were then subjected to the following cycle: 50°C for 2 min, 40x (95°C for 10 min, 95°C for 15 sec, 60°C for 1 min).

qPCR

The placenta was macerated in 1.5 mL of TRIzol reagent (Life Technologies, Thermo Fischer, USA). RNA extraction was performed following the manufacturer's protocol. cDNA was prepared using Power SYBR Green PCR Master Mix (Life Technologies, Thermo Fisher, USA). The reaction was carried out for selected genes using intron-spanning primers (**Table 2**) and the StepOnePlus Real-Time PCR system (Life Technologies, Thermo Fischer, USA). Samples were subjected to the following cycle: 95°C for 10 min followed by 40 amplification cycles consisting of DNA denaturation for 30 sec at 95°C and annealing of primers for 30 sec at 60°C. The threshold cycles (Ct) for each gene of interest and for the reference gene glycerol 3-phosphate dehydrogenase (*Gapdh*) and RNA Polymerase II Subunit A (*Polr2a)* were determined. The relative expression for each gene was calculated using $2^{-\Delta\Delta CT}$ (76) (Livak and Schmittgen 2001) and graphically expressed as the fold-increase. The efficiency was calculated using the standard curve method. The melting curves were analyzed for each sample.

Table 2: Primer sequences for the real-time PCR assay.

Gene	Primer sequences	GenBank accession no.

ZIKV	5'CCGCTGCCCAACACAAG3' 5'CCACTAACGTTCTTTTGCAGACAT3'	
mIL-6	5'TCATATCTTCAACCAAGAGGTA3' 5'CAGTGAGGAATGTCCACAAACTG3'	NM_031168.2
mIL-1b	5'GTAATGAAAGACGGCACACC3' 5'ATTAGAAACAGTCCAGCCCA3'	XM_006498795.4
mIL-10	5'TAAGGGTTACTTGGGTTGCCAAG3' 5'CAAATGCTCCTTGATTTCTGGGC3'	NM_010548.2
mIFN-γ	5'AGCAACAGCAAGGCGAAAA3' 5'CTGGACCTGTGGGTTGTTGA3'	NM_008337.4
m-IFN-I	5'CTGGAGCAGCTGAATGGAAAG3' 5'CTTGAAGTCCGCCCTGTAGGT3'	NM_010510.1
mGAPDH	5'CTTTGTCAAGCTCATTTCCTGG3' 5'TCTTGCTCAGTGTCCTTGC3'	XM_017321385.2
TNF-a	5'CCTCACACTCAGATCATCTTCTCA3' 5'TGGTTCTCTTTGAGATCCATGC3'	NM_013693.3
Polr2a	5'TCTGCCAAGAATGTGACGCT3' 5'CCAAGCGGCAAAGAATGTCC3'	NM_001291068.1

Detection of cytokines and chemokines in the maternal serum and placenta

Initially, placental tissue was homogenized in extraction buffer (50 mM Tris, 150 mM NaCl, 1X Triton, 0.1% SDS, 5 mM EDTA, 5 mM NaF, 50 mM sodium pyrophosphate, 1 mM sodium orthovanadate, pH 7.4) containing complete protease inhibitor cocktail (Roche Applied Science, Germany) with TissueLyser LT (Qiagen, Germany). The protein concentration of each sample was analyzed using the Pierce™ BCA Protein Assay Kit (Thermo Scientific, USA) according to the manufacturer's

instructions. Analysis of the cytokines IL-6 and IL1-β and the chemokines monocyte chemoattractant protein-1 (MCP-1/CCL2) and chemokine (C-X-C motif) ligand 1 (CXCL1) in maternal serum and placenta was performed with the MILLIPLEX MAP Mouse Cytokine/Chemokine Magnetic Bead Panel – Immunology Multiplex Assays (MCYTOMAG-70K, Merck Millipore, Germany), following the manufacturer's recommendations. The plate with samples and magnetic beads was analyzed on a MAGPIX® System (Merck Millipore, Germany). The analyses were performed using the Luminex xPonent® for MAGPIX® v software. 4.2 (Luminex Corp., USA). For each reaction well, the MAGPIX Luminex® platform reports the median fluorescence intensity (MFI) for each of the analytes in the samples. The levels of each analyte were then calculated against the standard curve. The ratio between the value obtained and the protein quantification for each sample was determined and plotted.

Virus titration by plaque assays

Blood from mock- and $ZIKV_{PE243}$-infected mice was collected from the base of the tail at 4 hours, 48 hours and 144 hours following the appropriate treatments and subsequently centrifuged at 400 g for 30 min for plasma separation. Samples obtained at different periods post infection were titrated by a plaque assay. Vero cells (obtained from ATCC® CCL81™) (African green monkey kidney epithelial cell line) were plated in 24-well plates at $4x10^4$ cells per well in DMEM (GIBCO, Thermo Fisher, USA) supplemented with 5% FBS (GIBCO, Thermo Fisher, USA) and 1% gentamicin (10 µg/ml) (GIBCO, Thermo Fisher, USA) and cultured overnight for complete adhesion at 37°C with 5% CO_2. Then, the medium was removed, and the cells were washed with 1x PBS and incubated with serial (base 10) dilutions of virus in FBS-free medium. After 90 min of incubation under gentle shaking, the medium was removed, and the cells were

washed with 1x PBS and cultured with 1.5% carboxymethylcellulose (CMC) supplemented with 1% FBS (GIBCO, Thermo Fisher, USA). After 5 days, the cells were fixed overnight with 4% formaldehyde and stained with 1% crystal violet in 20% methanol (ISOFAR, Brazil) for 1 hour. Plaques were counted, and the virus yield was calculated and expressed as plaque-forming units per milliliter (PFU/ml).

Histological, immunohistochemistry and TUNEL analyses of the placenta

Placental fragments were fixed overnight and subjected to dehydration (increasing ethanol series, ISOFAR, Brazil), diaphanization with xylol (ISOFAR, Brazil) and paraffin (Histopar, Easypath, Brazil). Sections (5 µm) were prepared using the Rotatory Microtome CUT 5062 (Slee Medical GmbH, Germany) and subjected to immunohistochemistry and TUNEL analyses.

For immunohistochemistry, blocking endogenous peroxidase was performed with 3% hydrogen peroxide diluted in PBS, followed by microwave antigenic recovery in Tris-EDTA (pH=9) and sodium citrate (pH=6) buffers (15 min for Tris-EDTA buffer and 8 min for citrate buffer). Sections were washed in PBS + 0.2% Tween and exposed to 3% PBS/BSA for 1 hour. Sections were then incubated overnight at 4°C with the following primary antibodies: anti-Ki-67 (1:100 – [M3064]; Spring Bioscience, USA), anti-P-gp (1:500 – Mdr1[sc-55510]; Santa Cruz Biotechnology, USA), anti-Bcrp (1:100 – Bcrp [MAB4146]; Merck Millipore, USA), anti-Abcg1 (1:100 – [PA5-13462]; Thermo Fisher Scientific, USA) or anti-Abca1 (1:100 – [ab18180]; Abcam Plc, UK). The next day, sections were incubated with the biotin-conjugated secondary antibody SPD-060 (Spring Bioscience, USA) for 1 hour at room temperature. Three washes were performed with PBS + 0.2% Tween followed by incubation with streptavidin (SPD-060 - Spring

Bioscience, USA) for 30 min. Sections were stained with 3,3-diamino-benzidine (DAB) (SPD-060 - Spring Bioscience, USA), counterstained with hematoxylin (Proquímios, Brazil), dehydrated, diaphanized and mounted with coverslip and entellan (Merck, Germany).

For analysis of apoptotic nuclei, terminal deoxynucleotidyl transferase dUTP nick-end labeling (TUNEL) staining was performed using the ApopTag® In Situ Peroxidase Detection Kit (S7100, Merck Millipore, USA) according to the manufacturer's recommendations and as previously described (65). All negative controls were performed with the omission of the primary antibody.

Image acquisition was performed using a high-resolution Olympus DP72 (Olympus Corporation, Japan) camera coupled to an Olympus BX53 light microscope (Olympus Corporation, Japan). For nuclear quantification of Ki-67 and TUNEL immunolabeling, Stepanizer software (77) was used. For this analysis, we evaluated 15 images from different random fields of the Lz and Jz for each animal, in a total of five animals from each ICompetent group and three animals from each ICompromised group. A total of 360 digital images per placental region (Lz and Jz) were evaluated in each experimental group. Total numbers of immunolabeled Ki-67 or TUNEL nuclei from each image were normalized by the total image area to obtain an index of estimated numbers of proliferative and apoptotic nuclei in the whole histological section analyzed. Analysis was undertaken by two investigators blinded to the treatment.

Quantification of P-gp, Bcrp, Abca1 and Abcg1 staining was performed using the Image-Pro Plus, version 5.0 software (Media Cybernetics, USA) mask tool. The percentage of viable tissue area was considered upon exclusion of negative spaces. A total

of 360 digital images per placental region (Lz and Jz) were evaluated in each experimental group. Analysis was undertaken by two investigators blinded to the treatment.

Transmission electron microscopy (TEM)

Sections of placental Lz and Jz were fixed in paraformaldehyde (4%, Sigma-Aldrich, Brazil) for 48 hours, postfixed with osmium tetroxide (Electron Microscopy Sciences, USA) and potassium ferrocyanide (Electron Microscopy Sciences, USA) for 60 min and dehydrated with an increasing series of acetone (30%, 50%, 70%, 90% and two of 100%) (ISOFAR, Brazil). Sections were subsequently embedded with EPOXI resin (Electron Microscopy Sciences, USA) and acetone (1:2, 1:1 and 2:1, respectively). After polymerization, ultrafine sections (70 nm) were prepared (Leica Microsystems, USA) and collected into 300 mesh copper grids (Electron Microscopy Sciences, USA). Tissue was contrasted with uranyl acetate and lead citrate and visualized using a JEOL JEM-1011 transmission electron microscope (JEOL, Ltd., Akishima, Tokyo, Japan). Digital micrographs were captured using an ORIUS CCD digital camera (Gatan, Inc., Pleasanton, California, EUA) at 6000× magnification. An overall qualitative analysis of Lz and Jz from different groups was performed by investigating the ultrastructural characteristics of the mitochondria as well as the ER cisterns. The qualitative evaluation consisted of analyzing the disruption of the mitochondrial membranes, mitochondrial morphology, preservation of mitochondrial cristae and matrix intensity (78). Ultrastructural analysis of nuclear morphology and the presence of microvilli in trophoblast sinusoidal giant cells was also undertaken. The analysis of the cisterns of the ER was performed by evaluating the dilation of their lumen (55).

Statistical analysis

GraphPad Prism 8 software (GraphPad Software, Inc., USA) was used for statistical analysis. The D'Agostino & Pearson normality test was used to evaluate normal distribution, and outliers were identified using the Grubbs test. Data are expressed as the mean ±SEM or individual values. One-way ANOVA followed by Tukey's posttest was used for comparisons between different inbred groups, whereas Student's t-test or nonparametric Mann-Whitney test was performed between the outbred groups. Differences were considered significant when $p<0.05$. Pregnancy parameters were evaluated using the mean value of all fetuses and placentae in a litter per dam and not the individual conceptus, i.e., the mean value. "n" represents the number of litters in Figures 1 and 2 (49,65,74).

Acknowledgments

We would like to thank Alan Moraes for supporting the acquisition of electron microscopy images and the electron microscopy laboratory at the UFF Biology Institute for allowing the use of the JEM1011 transmission electron microscope. Mauro Jorge Castro Cabral for the use of the MAGPIX® System equipment from the Paulo de Góes Institute of Microbiology/UFRJ. Ernesto T. Marques Jr. (Centro de Pesquisa Aggeu Magalhães, FIOCRUZ, PE) for providing ZIKV to the Institute of Microbiology Paulo de Góes, Federal University of Rio de Janeiro and the technicians Juliana Gonçalves and Rakel Alves for their support during all the experiments.

Financial support

This study was supported by the Bill & Melinda Gates Foundation (MCTI/CNPq/MS/SCTIE/Decit/Bill and Melinda Gates 05/2013; OPP1107597), the Canadian Institutes for Health Research (SGM: Foundation-148368), Conselho Nacional de Desenvolvimento Científico e Tecnológico (CNPq; 304667/2016-1, 422441/2016-3, 303734/2012-4, 422410/2016-0), Coordenação de Aperfeiçoamento Pessoal de Nível Superior (CAPES, finance Code 001), Fundação de Amparo à Pesquisa do Estado do Rio de Janeiro (FAPERJ, CNE 2015/E26/203.190/2015, PDR-26/2002/010/2016), and PRPq-Universidade MG Federal MGPEFARJ, CNE 2015/E26/203.190/2015).

References

1. Garcez PP, Loiola EC, Madeiro da Costa R, Higa LM, Trindade P, Delvecchio R, et al. Zika virus impairs growth in human neurospheres and brain organoids. Science. 2016;352(6287):816–8.
2. Brasil P, Calvet GA, Siqueira AM, Wakimoto M, de Sequeira PC, Nobre A, et al. Zika Virus Outbreak in Rio de Janeiro, Brazil: Clinical Characterization, Epidemiological and Virological Aspects. Powers AM, editor. PLoS Negl Trop Dis. 2016;10(4):e0004636.
3. Brasil P, Nielsen-Saines K. More pieces to the microcephaly–Zika virus puzzle in Brazil. The Lancet Infectious Diseases. 2016;16(12):1307–9.
4. Brasil P, Pereira JP, Moreira ME, Ribeiro Nogueira RM, Damasceno L, Wakimoto M, et al. Zika Virus Infection in Pregnant Women in Rio de Janeiro. N Engl J Med. 2016 Mar 4;375(24):2321–34.
5. Jaenisch T, Rosenberger KD, Brito C, Brady O, Brasil P, Marques ET. Risk of microcephaly after Zika virus infection in Brazil, 2015 to 2016. Bull World Health Organ. 2017;95(3):191–8.
6. Proenca-Modena JL, Milanez GP, Costa ML, Judice CC, Maranhão Costa FT. Zika virus: lessons learned in Brazil. Microbes and Infection. 2018;20(11–12):661–9.
7. Jouannic J-M, Friszer S, Leparc-Goffart I, Garel C, Eyrolle-Guignot D. Zika virus infection in French Polynesia. The Lancet. 2016;387(10023):1051–2.
8. Musso D, Ko AI, Baud D. Zika Virus Infection — After the Pandemic. Longo DL, editor. N Engl J Med. 2019;381(15):1444–57.
9. Kasprzykowski JI, Fukutani KF, Fabio H, Fukutani ER, Costa LC, Andrade BB, et al. A recursive sub-typing screening surveillance system detects the appearance of the ZIKV African lineage in Brazil: Is there a risk of a new epidemic? International Journal of Infectious Diseases. 2020;96:579–81.
10. Miranda J, Martín-Tapia D, Valdespino-Vázquez Y, Alarcón L, Espejel-Nuñez A, Guzmán-Huerta M, et al. Syncytiotrophoblast of Placentae from Women with Zika

Virus Infection Has Altered Tight Junction Protein Expression and Increased Paracellular Permeability. Cells. 2019;8(10):1174.
11. Jurado KA, Simoni MK, Tang Z, Uraki R, Hwang J, Householder S, et al. Zika virus productively infects primary human placenta-specific macrophages. JCI Insight. 2016;1(13):e88461.
12. Quicke KM, Bowen JR, Johnson EL, McDonald CE, Ma H, O'Neal JT, et al. Zika Virus Infects Human Placental Macrophages. Cell Host & Microbe. 2016;20(1):83–90.
13. Tabata T, Petitt M, Puerta-Guardo H, Michlmayr D, Wang C, Fang-Hoover J, et al. Zika Virus Targets Different Primary Human Placental Cells, Suggesting Two Routes for Vertical Transmission. Cell Host & Microbe. 2016;20(2):155–66.
14. Simoni MK, Jurado KA, Abrahams VM, Fikrig E, Guller S. Zika virus infection of Hofbauer cells. Am J Reprod Immunol. 2017;77(2):e12613.
15. Lazear HM, Govero J, Smith AM, Platt DJ, Fernandez E, Miner JJ, et al. A Mouse Model of Zika Virus Pathogenesis. Cell Host & Microbe. 2016;19(5):720–30.
16. Grant A, Ponia SS, Tripathi S, Balasubramaniam V, Miorin L, Sourisseau M, et al. Zika Virus Targets Human STAT2 to Inhibit Type I Interferon Signaling. Cell Host & Microbe. 2016;19(6):882–90.
17. Yockey LJ, Varela L, Rakib T, Khoury-Hanold W, Fink SL, Stutz B, et al. Vaginal Exposure to Zika Virus during Pregnancy Leads to Fetal Brain Infection. Cell. 2016;166(5):1247-1256.e4.
18. Garcez PP, Stolp HB, Sravanam S, Christoff RR, Ferreira JCCG, Dias AA, et al. Zika virus impairs the development of blood vessels in a mouse model of congenital infection. Sci Rep. 2018;8(1):12774.
19. Elong Ngono A, Shresta S. Immune Response to Dengue and Zika. Annu Rev Immunol. 2018;36(1):279–308.
20. Bayer A, Lennemann NJ, Ouyang Y, Bramley JC, Morosky S, Marques ETDAJ, et al. Type III Interferons Produced by Human Placental Trophoblasts Confer Protection against Zika Virus Infection. Cell Host Microbe. 2016;19(5):705–12.
21. Luo H, Winkelmann ER, Fernandez-Salas I, Li L, Mayer SV, Danis-Lozano R, et al. Zika, dengue and yellow fever viruses induce differential anti-viral immune responses in human monocytic and first trimester trophoblast cells. Antiviral Research. 2018;151:55–62.
22. Tanaka T, Narazaki M, Kishimoto T. IL-6 in Inflammation, Immunity, and Disease. Cold Spring Harb Perspect Biol. 2014;6(10):a016295.
23. Hunter CA, Jones SA. IL-6 as a keystone cytokine in health and disease. Nature Immunology. 2015;16(5):448–57.
24. Rabelo K, Gonçalves AJ da S, Souza LJ de, Sales AP, Lima SMB de, Trindade GF, et al. Zika Virus Infects Human Placental Mast Cells and the HMC-1 Cell Line, and Triggers Degranulation, Cytokine Release and Ultrastructural Changes. Cells. 2020;9(4):975–90.
25. Bloise E, Ortiga-Carvalho TM, Reis FM, Lye SJ, Gibb W, Matthews SG. ATP-binding cassette transporters in reproduction: a new frontier. Hum Reprod Update. 2015;22(2):164–81.
26. do Imperio GE, Bloise E, Javam M, Lye P, Constantinof A, Dunk C, et al. Chorioamnionitis Induces a Specific Signature of Placental ABC Transporters Associated with an Increase of miR-331-5p in the Human Preterm Placenta. Cell Physiol Biochem. 2018;45(2):591–604.

27. Martinelli LM, Fontes KN, Reginatto MW, Andrade CBV, Monteiro VRS, Gomes HR, et al. Malaria in pregnancy regulates P-glycoprotein (P-gp/Abcb1a) and ABCA1 efflux transporters in the mouse visceral yolk sac. J Cell Mol Med. 2020;00:1–12.
28. Martinelli LM, Reginatto MW, Fontes KN, Andrade CBV, Monteiro VRS, Gomes HR, et al. Breast cancer resistance protein (Bcrp/Abcg2) is selectively modulated by lipopolysaccharide (LPS) in the mouse yolk sac. Reprod Toxicol. 2020 Sep 8 [cited 2020 Oct 8]
29. Reginatto MW, Fontes KN, Monteiro VRS, Silva NL, Andrade CBV, Gomes HR, et al. Effect of sub-lethal prenatal endotoxemia on murine placental transport systems and lipid homeostasis. bioRxiv. 2020 Aug 5;2020.08.04.236745.
30. Imperio GE, Javam M, Lye P, Constantinof A, Dunk CE, Reis FM, et al. Gestational age-dependent gene expression profiling of ATP-binding cassette transporters in the healthy human placenta. J Cell Mol Med. 2018/11/08 ed. 2019;23(1):610–8.
31. Vermillion MS, Lei J, Shabi Y, Baxter VK, Crilly NP, McLane M, et al. Intrauterine Zika virus infection of pregnant immunocompetent mice models transplacental transmission and adverse perinatal outcomes. Nat Commun. 2017;8(1):14575.
32. Szaba FM, Tighe M, Kummer LW, Lanzer KG, Ward JM, Lanthier P, et al. Zika virus infection in immunocompetent pregnant mice causes fetal damage and placental pathology in the absence of fetal infection. Coyne CB, editor. PLoS Pathog. 2018;14(4):e1006994.
33. Hamilton SA, Tower CL, Jones RL. Identification of Chemokines Associated with the Recruitment of Decidual Leukocytes in Human Labour: Potential Novel Targets for Preterm Labour. PLOS ONE. 2013 Feb 22;8(2):e56946.
34. Bloise E, Bhuiyan M, Audette MC, Petropoulos S, Javam M, Gibb W, et al. Prenatal Endotoxemia and Placental Drug Transport in The Mouse: Placental Size-Specific Effects. PLOS ONE. 2013 Jun 10;8(6):e65728.
35. Romero R, Mazor M, Brandt F, Sepulveda W, Avila C, Cotton DB, et al. Interleukin-1α and Interleukin-1 β in Preterm and Term Human Parturition. American Journal of Reproductive Immunology. 1992;27(3-4):117–23.
36. Larocca RA, Abbink P, Peron JPS, de A. Zanotto PM, Iampietro MJ, Badamchi-Zadeh A, et al. Vaccine protection against Zika virus from Brazil. Nature. 2016;536(7617):474–8.
37. Souza IN de O, Frost PS, França JV, Nascimento-Viana JB, Neris RLS, Freitas L, et al. Acute and chronic neurological consequences of early-life Zika virus infection in mice. Science Translational Medicine. 2018;10(444):eaar2749.
38. Kalagiri RR, Carder T, Choudhury S, Vora N, Ballard AR, Govande V, et al. Inflammation in Complicated Pregnancy and Its Outcome. Am J Perinatol. 2016;33(14):1337–56.
39. Barbeito-Andrés J, Pezzuto P, Higa LM, Dias AA, Vasconcelos JM, Santos TMP, et al. Congenital Zika syndrome is associated with maternal protein malnutrition. Sci Adv. 2020;6(2):eaaw6284.
40. Saito S, Nakashima A, Shima T, Ito M. REVIEW ARTICLE: Th1/Th2/Th17 and Regulatory T-Cell Paradigm in Pregnancy. American Journal of Reproductive Immunology. 2010;63(6):601–10.
41. Gotsch F, Romero R, Kusanovic JP, Mazaki-Tovi S, Pineles BL, Erez O, et al. The fetal inflammatory response syndrome. Clin Obstet Gynecol. 2007;50(3):652–83.

42. Galinsky R, Polglase GR, Hooper SB, Black MJ, Moss TJM. The consequences of chorioamnionitis: preterm birth and effects on development. J Pregnancy. 2013;2013:412831.
43. Mor G, Cardenas I, Abrahams V, Guller S. Inflammation and pregnancy: the role of the immune system at the implantation site. Ann N Y Acad Sci. 2011;1221(1):80–7.
44. Bradley MP, Nagamine CM. Animal Models of Zika Virus. Comparative Medicine. 2017;67(3):242–52.
45. Novembri R, Torricelli M, Bloise E, Conti N, Galeazzi LR, Severi FM, et al. Effects of urocortin 2 and urocortin 3 on IL-10 and TNF-α expression and secretion from human trophoblast explants. Placenta. 2011;32(12):969–74.
46. Fortunato SJ, Menon R, Lombardi SJ. Interleukin-10 and transforming growth factor-beta inhibit amniochorion tumor necrosis factor-alpha production by contrasting mechanisms of action: therapeutic implications in prematurity. Am J Obstet Gynecol. 1997;177(4):803–9.
47. Chatterjee P, Chiasson VL, Bounds KR, Mitchell BM. Regulation of the Anti-Inflammatory Cytokines Interleukin-4 and Interleukin-10 during Pregnancy. Front Immunol. 2014;5(253):1–6.
48. Bloise E, Torricelli M, Novembri R, Borges LE, Carrarelli P, Reis FM, et al. Heat-killed Lactobacillus rhamnosus GG Modulates Urocortin and Cytokine Release in Primary Trophoblast Cells. Placenta. 2010;31(10):867–72.
49. Connor KL, Kibschull M, Matysiak-Zablocki E, Nguyen TT-TN, Matthews SG, Lye SJ, et al. Maternal malnutrition impacts placental morphology and transporter expression: an origin for poor offspring growth. The Journal of Nutritional Biochemistry. 2020;78:108329.
50. Ribeiro MR, Moreli JB, Marques RE, Papa MP, Meuren LM, Rahal P, et al. Zika-virus-infected human full-term placental explants display pro-inflammatory responses and undergo apoptosis. Arch Virol. 2018;163(10):2687–99.
51. Gown AM, Willingham MC. Improved Detection of Apoptotic Cells in Archival Paraffin Sections: Immunohistochemistry Using Antibodies to Cleaved Caspase 3. J Histochem Cytochem. 2002;50(4):449–54.
52. Noronha L de, Zanluca C, Burger M, Suzukawa AA, Azevedo M, Rebutini PZ, et al. Zika Virus Infection at Different Pregnancy Stages: Anatomopathological Findings, Target Cells and Viral Persistence in Placental Tissues. Front Microbiol. 2018;9(2266):1–11.
53. Offerdahl DK, Dorward DW, Hansen BT, Bloom ME. Cytoarchitecture of Zika virus infection in human neuroblastoma and Aedes albopictus cell lines. Virology. 2017;501:54–62.
54. Lojpur T, Easton Z, Raez-Villanueva S, Laviolette S, Holloway AC, Hardy DB. Δ9-Tetrahydrocannabinol leads to endoplasmic reticulum stress and mitochondrial dysfunction in human BeWo trophoblasts. Reproductive Toxicology. 2019;87:21–31.
55. Montalbano R, Waldegger P, Quint K, Jabari S, Neureiter D, Illig R, et al. Endoplasmic Reticulum Stress Plays a Pivotal Role in Cell Death Mediated by the Pan-Deacetylase Inhibitor Panobinostat in Human Hepatocellular Cancer Cells. Translational Oncology. 2013;6(2):143-IN6.
56. Desuzinges-Mandon E, Arnaud O, Martinez L, Huché F, Di Pietro A, Falson P. ABCG2 Transports and Transfers Heme to Albumin through Its Large Extracellular Loop. J Biol Chem. 2010;285(43):33123–33.

57. Ledur PF, Karmirian K, Pedrosa C da SG, Souza LRQ, Assis-de-Lemos G, Martins TM, et al. Zika virus infection leads to mitochondrial failure, oxidative stress and DNA damage in human iPSC-derived astrocytes. Scientific Reports. 2020;10(1):1218.
58. Reemst K, Noctor SC, Lucassen PJ, Hol EM. The Indispensable Roles of Microglia and Astrocytes during Brain Development. Front Hum Neurosci [Internet]. 2016 [cited 2020 Jul 12];10.
59. Guitart-Mampel M, Gonzalez-Tendero A, Niñerola S, Morén C, Catalán-Garcia M, González-Casacuberta I, et al. Cardiac and placental mitochondrial characterization in a rabbit model of intrauterine growth restriction. Biochimica et Biophysica Acta (BBA) - General Subjects. 2018;1862(5):1157–67.
60. Guitart-Mampel M, Juarez-Flores DL, Youssef L, Moren C, Garcia-Otero L, Roca-Agujetas V, et al. Mitochondrial implications in human pregnancies with intrauterine growth restriction and associated cardiac remodelling. J Cell Mol Med. 2019;23(6):3962–73.
61. Zhang Z, Rong L, Li Y-P. Flaviviridae Viruses and Oxidative Stress: Implications for Viral Pathogenesis. Oxid Med Cell Longev. 2019;2019:1409582.
62. Martínez F, Kiriakidou M, Strauss JF. Structural and Functional Changes in Mitochondria Associated with Trophoblast Differentiation: Methods to Isolate Enriched Preparations of Syncytiotrophoblast Mitochondria. Endocrinology. 1997;138(5):2172–83.
63. Burton GJ, Yung HW, Murray AJ. Mitochondrial – Endoplasmic reticulum interactions in the trophoblast: Stress and senescence. Placenta. 2017;52:146–55.
64. Holland O, Dekker Nitert M, Gallo LA, Vejzovic M, Fisher JJ, Perkins AV. Review: Placental mitochondrial function and structure in gestational disorders. Placenta. 2017;54:2–9.
65. Fontes KN, Reginatto MW, Silva NL, Andrade CBV, Bloise FF, Monteiro VRS, et al. Dysregulation of placental ABC transporters in a murine model of malaria-induced preterm labor. Sci Rep. 2019;9(1):11488.
66. Bridges CC, Zalups RK, Joshee L. Toxicological significance of renal Bcrp: Another potential transporter in the elimination of mercuric ions from proximal tubular cells. Toxicol Appl Pharmacol. 2015;285(2):110–7.
67. Szilagyi JT, Gorczyca L, Brinker A, Buckley B, Laskin JD, Aleksunes LM. Placental BCRP/ABCG2 Transporter Prevents Fetal Exposure to the Estrogenic Mycotoxin Zearalenone. Toxicol Sci. 2019;168(2):394–404.
68. Scialis RJ, Aleksunes LM, Csanaky IL, Klaassen CD, Manautou JE. Identification and Characterization of Efflux Transporters That Modulate the Subtoxic Disposition of Diclofenac and Its Metabolites. Drug Metab Dispos. 2019;47(10):1080–92.
69. Mao Q, Unadkat JD. Role of the breast cancer resistance protein (BCRP/ABCG2) in drug transport--an update. AAPS J. 2015;17(1):65–82.
70. Lye P, Bloise E, Javam M, Gibb W, Lye SJ, Matthews SG. Impact of Bacterial and Viral Challenge on Multidrug Resistance in First- and Third-Trimester Human Placenta. The American Journal of Pathology. 2015;185(6):1666–75.
71. Girard S, Sebire G. Transplacental Transfer of Interleukin-1 Receptor Agonist and Antagonist Following Maternal Immune Activation. American journal of reproductive immunology (New York, NY : 1989). 2016;75(1):8–12.
72. Bloise E, Petropoulos S, Iqbal M, Kostaki A, Ortiga-Carvalho TM, Gibb W, et al. Acute Effects of Viral Exposure on P-Glycoprotein Function in the Mouse Fetal Blood-

Brain Barrier. Cellular physiology and biochemistry : international journal of experimental cellular physiology, biochemistry, and pharmacology. 2017;41(3):1044–50.
73. Coelho SVA, Neris RLS, Papa MP, Schnellrath LC, Meuren LM, Tschoeke DA, et al. Development of standard methods for Zika virus propagation, titration, and purification. Journal of Virological Methods. 2017;246:65–74.
74. Bloise E, Lin W, Liu X, Simbulan R, Kolahi KS, Petraglia F, et al. Impaired Placental Nutrient Transport in Mice Generated by *in Vitro* Fertilization. Endocrinology. 2012;153(7):3457–67.
75. Lanciotti RS, Kosoy OL, Laven JJ, Velez JO, Lambert AJ, Johnson AJ, et al. Genetic and Serologic Properties of Zika Virus Associated with an Epidemic, Yap State, Micronesia, 2007. Emerg Infect Dis. 2008 Aug;14(8):1232–9.
76. Livak KJ, Schmittgen TD. Analysis of Relative Gene Expression Data Using Real-Time Quantitative PCR and the 2−ΔΔCT Method. Methods. 2001;25(4):402–8.
77. Tschanz SA, Burri PH, Weibel ER. A simple tool for stereological assessment of digital images: the STEPanizer: TOOL FOR STEREOLOGICAL ASSESSMENT. Journal of Microscopy. 2011;243(1):47–59.
78. Sesso A, Belizário JE, Marques MM, Higuchi ML, Schumacher RI, Colquhoun A, et al. Mitochondrial Swelling and Incipient Outer Membrane Rupture in Preapoptotic and Apoptotic Cells. Anatomical Record (Hoboken, N.j : 2007). 2012 Oct;295(10):1647.

Figure Captions

Figure 1: ZIKV infection induced fetal changes during pregnancy. A) Experimental schematic. The fetuses from C57BL/6 dams and sires were termed ICompetent. The fetuses from the mates of A129 dams and C57BL/6 sires were termed ICompromised. B) Uterine horn images and survival images (arrows show resorption sites). C) Fetal/reabsorption images. Measurement of fetal biometric parameters at GD18.5. D) Fetal weight, (E) fetal head weight and (F) fetal head weight/fetal weight ratio in ICompetent (n=11/15/9 dams in the mock, high and low groups, respectively) and ICompromised (n=3 dams/group). * example reabsorption. The values are plotted as individual values, and the bar represents the mean. Unpaired Student's t-test or nonparametric Mann-Whitney test was used for ICompromised groups, and one-way ANOVA followed by Tukey's post-test was used for ICompetent comparisons between different groups.

Figure 2: Viral load present in the spleen, placenta, fetal and maternal brains after ZIKV infection. A) Maternal spleen and brain viral load and B) placenta and fetal brain viral load of ZIKV-infected dams. C) Animal viral serology of all groups after 4, 48 and 144 infection hours. ICompetent (n=11/15/9 dams in the mock, high and low ZIKV titer groups, respectively) and ICompromised (n=3 dams/group).

Figure 3: ZIKV promotes an inflammatory response in the placenta, maternal spleen and serum during pregnancy.

A) Cytokine and chemokine serum levels at GD18.5 in the ICompetent mock (n=9 dams), high (n=8) and low (n=9) and ICompromised mock and low (n=3/groups) ZIKV titer groups. A-C) IL-1β, IL-6, CCL-2 and CXCL-1 maternal serum levels. D-F) Placental IL-1β, IL-6, CCL-2 and CXCL-1 levels. G-I) Placental RNA levels of Ifnγ, *Ifn1, Il-1β, Il-6 and Tnf-α*. The broken line shows the expression levels of both lineages in the mock group. The values are expressed as the mean ± SEM. Unpaired Student's t-test or

nonparametric Mann-Whitney test was used for comparisons between ICompetent groups, and one-way ANOVA followed by Tukey's posttest was used for comparisons between different ICompetent groups. * $p<0.05$.

Figure 4: Placental remodeling of ICompetent groups induced by ZIKV infection. A) Quantification of Ki-67$^+$ nuclei in the mouse placenta Lz and representative images of nuclei immunostained by Ki-67$^+$-positive nuclei in the ICompetent group (n=6/group). B) The image shows the apoptotic nuclei score in the Lz and representative images of nuclei immunostained by TUNEL in the ICompetent group (n=5/group). C) Quantification of Ki-67+ nuclei in the mouse placenta Lz and representative images of nuclei immunostained by Ki-67$^+$ nuclei in the ICompromised group (n=3/group). D) The image shows the apoptotic nuclei score in the LZ and representative images of nuclei immunostained by TUNEL in the ICompromised group (n=3/group). The values are expressed as the mean ± SEM. One-way ANOVA followed by Tukey's post hoc test was used for comparisons between different ICompetent groups. Unpaired Student's t-tests or nonparametric Mann-Whitney tests were used for the ICompromised groups. CTR(-)=All negative controls were performed with the omission of the primary antibody. Scale bar = 50 µm.

Figure 5: ZIKV induces hyperproliferation of the JZ area in infected placentas of ICompetent groups. A) Quantification of Ki-67+ nuclei in the placental Jz of mice and representative images of immunostained nuclei in the ICompetent (n=6/group). B) The image shows apoptotic nuclei quantification in the Jz area and representative images of nuclei immunostained by TUNEL in the ICompetent (n=5/group). C) Quantification of Ki-67+ nuclei in the placental Jz area and representative images of immunostained nuclei in the ICompromised group (n=3/group). D) The image shows apoptotic nuclei quantification in the Jz area and representative images of nuclei immunostained by TUNEL in the ICompromised (n=3/group). The values are expressed as the mean ± SEM. One-way ANOVA followed by Tukey's post hoc test was used for comparisons between different ICompetent groups. Unpaired Student's t-tests or nonparametric Mann-Whitney tests were used for the ICompromised groups. CTR(-)=All negative controls were performed with the omission of the primary antibody. Scale bar = 50 µm.

Figure 6: Associated ultrastructural changes in the placental LZ after ZIKV infection. Transmission electron photomicrographs of ICompetent mock (A); ICompetent high (B); ICompetent low (C); ICompromised mock (D) and ICompromised low (E) groups (N=5 dams/group). We observed dilatation in the ER cisterns of ICompetent high placentas. Additionally, there was a reduction in the microvilli from both ICompetent high and ICompetent low placentas. In the ICompromised low group, we found fragmented ER and microvillus reduction. All infected groups showed degenerate mitochondria. GER= Granular Endoplasmic Reticulum; Δ= Dilated Granular Endoplasmic Reticulum; *= Fragmented Granular Endoplasmic Reticulum; Mt= Mitochondria; MtD= Degenerate Mitochondria; Mv= Microvilli; EN= Euchromatic Nuclei; SS= Sinusoidal Space; TGC= Trophoblastic Giant Cell. Scale bar = 2 µm.

Figure 7: Associated ultrastructural changes in the placental JZ after ZIKV infection. Transmission electron photomicrographs of ICompetent mock (A);

ICompetent high (B); ICompetent low (C); ICompromised mock (D) and ICompromised low (E) groups (N=5 dams/group). We found deteriorating mitochondria and dilated reticulum endoplasmic cisterns in both the high ICompetent and low ICompromised groups. GER= Granular Endoplasmic Reticulum; Δ= Dilated Granular Endoplasmic Reticulum; Mt= Mitochondria; MtD= Degenerate Mitochondria; Mv= Microvilli; EN= Euchromatic Nuclei; SS= Sinusoidal Space; TGC= Trophoblastic Giant Cell. White arrows HA = Heterochromatin Area. Scale bar = 2 µm.

Figure 8: ZIKV infection decreases P-gp, Bcrp and Abca1 expression in the placental LZ of infected mice in the ICompetent groups. Immunostaining quantification and representative immunohistochemistry images of A) P-gp, B) Bcrp, C) Abca1 and D) Abcg1. The images represent the percentage of stained cells in each analyzed field. The values are expressed as the mean ± SEM. One-way ANOVA followed by Tukey's post hoc test was used for comparisons between different ICompetent groups. Scale bar = 50 µm. N=6/ group. CTR(-)=All negative controls were performed with the omission of the primary antibody.

Figure 9: ZIKV infection decreases P-gp, Bcrp and Abca protein expression in the placental LZ of infected mice in the ICompromised groups. Immunostaining quantification and representative immunohistochemistry images of A) P-gp, B) Bcrp, C) Abca1 and D) Abcg1. The images represent the percentage of stained cells in each analyzed field. The values are expressed as the mean ± SEM. Unpaired Student's t-tests or nonparametric Mann-Whitney tests were used for the ICompromised groups. Scale bar = 50 µm. N=3 for each group. CTR(-)=All negative controls were performed with the omission of the primary antibody.

Figure 10: ZIKV infection did not impact P-gp, Bcrp, Abca1 or ABcg1 expression in the JZ area in infected placentas of ICompetent groups. Immunostaining quantification and representative immunohistochemistry images of A) P-gp, B) Bcrp, C) Abca1 and D) Abcg1. The images represent the percentage of stained cells/viable tissue. The values are expressed as the mean ± SEM. One-way ANOVA followed by Tukey's post hoc test was used for comparisons between different ICompetent groups. Scale bar = 50 µm. N=6/each group. CTR(-)=All negative controls were performed with the omission of the primary antibody.

Figure 11: ZIKV infection decreases Bcrp expression in the JZ area in infected placentas of the ICompromised group. Immunostaining quantification and representative immunohistochemistry images of A) P-gp, B) Bcrp, C) Abca1 and D) Abcg1. The images represent the percentage of stained cells/viable tissue. The values are expressed as the mean ± SEM. Unpaired Student's t-tests or nonparametric Mann-Whitney tests were used for the ICompromised groups. Scale bar = 50 µm. N=3 for each group. CTR(-)=All negative controls were performed with the omission of the primary antibody.

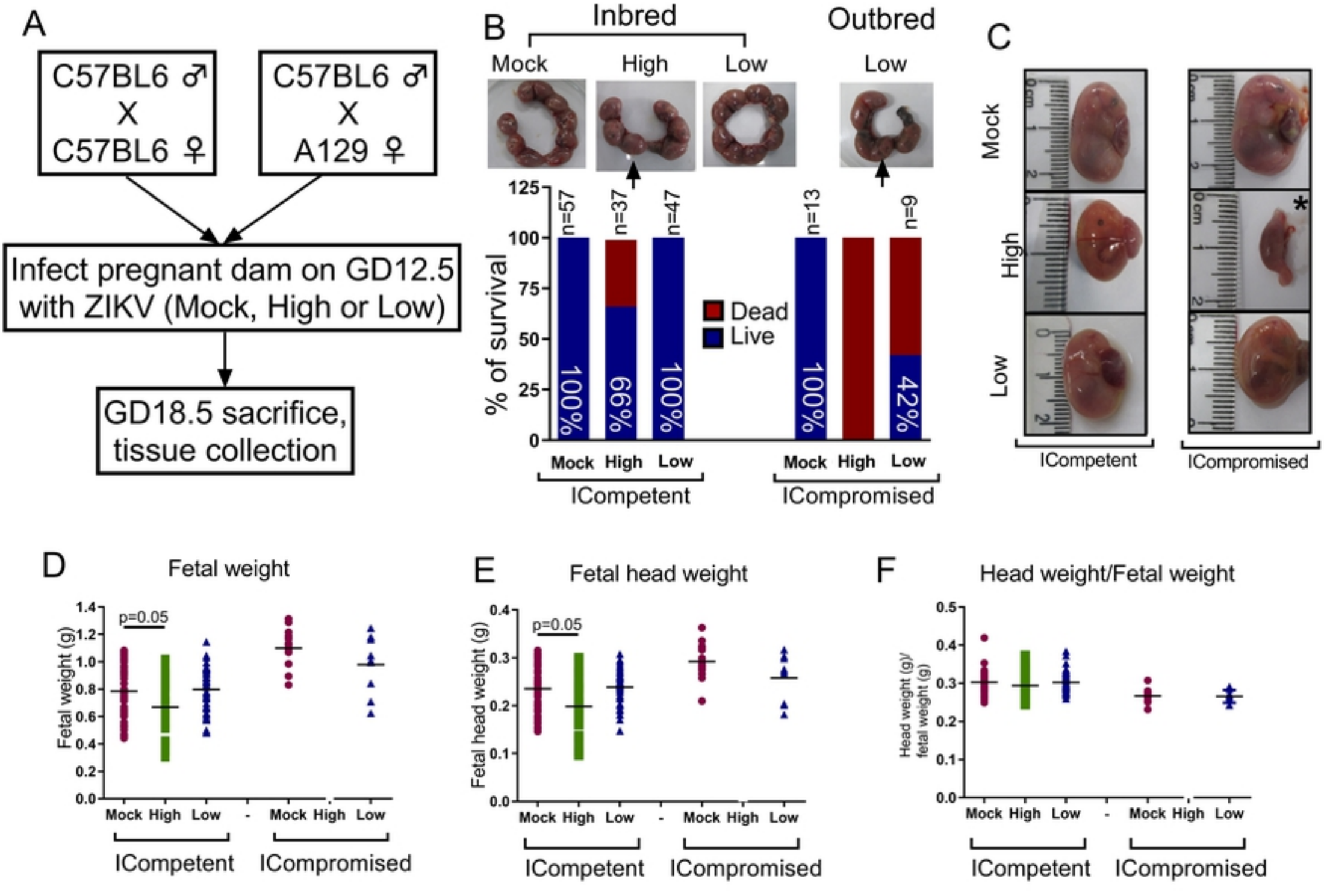
A
C57BL6 ♂ X C57BL6 ♀
C57BL6 ♂ X A129 ♀
Infect pregnant dam on GD12.5 with ZIKV (Mock, High or Low)
GD18.5 sacrifice, tissue collection
B
Inbred
Outbred
Mock
High
Low
Low
% of survival
n=57
n=37
n=47
n=13
n=9
100%
66%
100%
100%
42%
Dead
Live
Mock High Low
Mock High Low
ICompetent
ICompromised
C
Mock
High
Low
ICompetent
ICompromised
D
Fetal weight
p=0.05
Fetal weight (g)
Mock High Low - Mock High Low
ICompetent ICompromised
E
Fetal head weight
p=0.05
Fetal head weight (g)
Mock High Low - Mock High Low
ICompetent ICompromised
F
Head weight/Fetal weight
Head weight (g)/ fetal weight (g)
Mock High Low - Mock High Low
ICompetent ICompromised

Figure 1

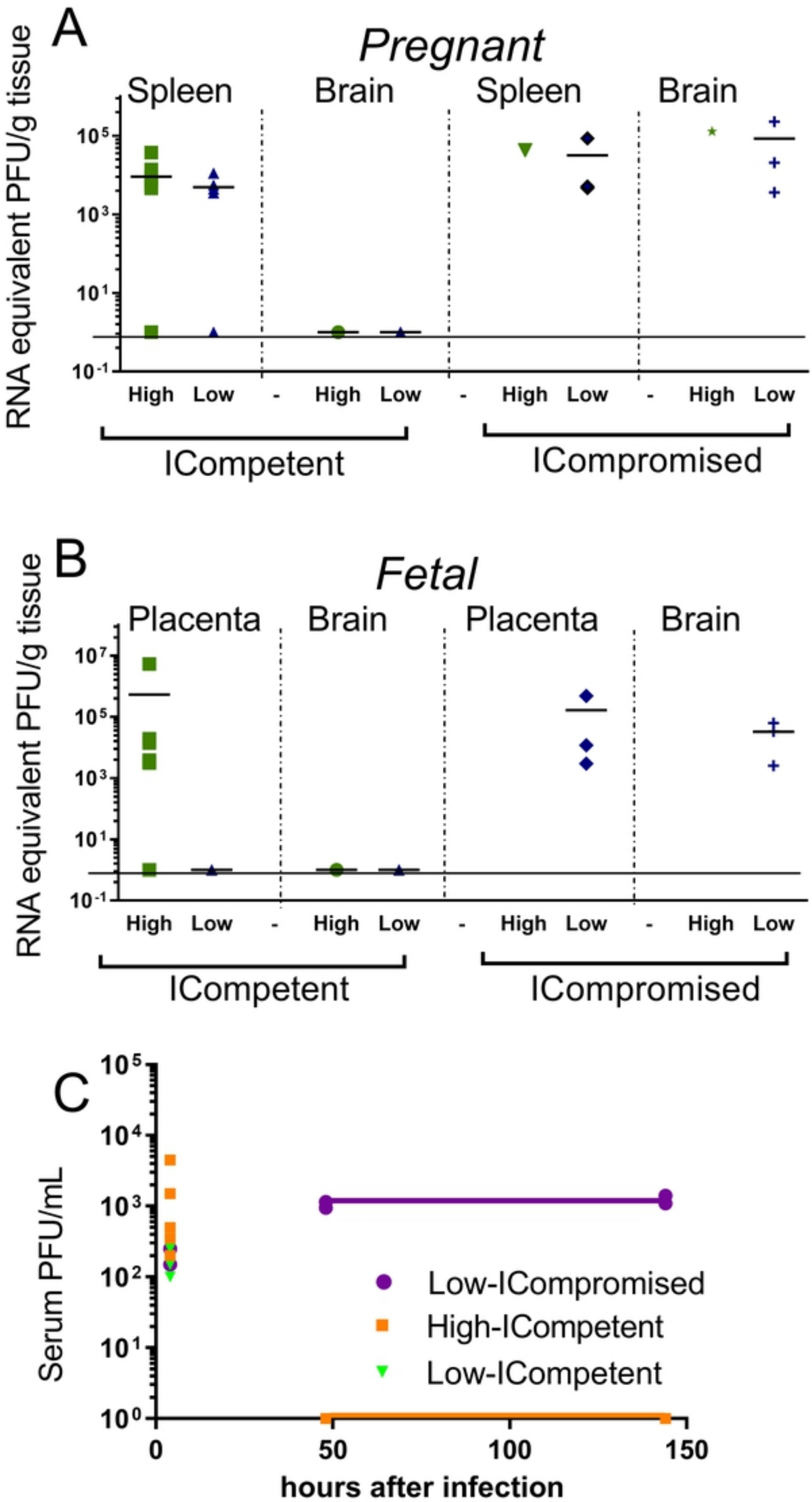
A
Pregnant
Spleen
Brain
Spleen
Brain
RNA equivalent PFU/g tissue
High
Low
-
High
Low
-
High
Low
-
High
Low
ICompetent
ICompromised
B
Fetal
Placenta
Brain
Placenta
Brain
RNA equivalent PFU/g tissue
High
Low
-
High
Low
-
High
Low
-
High
Low
ICompetent
ICompromised
C
Serum PFU/mL
Low-ICompromised
High-ICompetent
Low-ICompetent
hours after infection

Figure 2

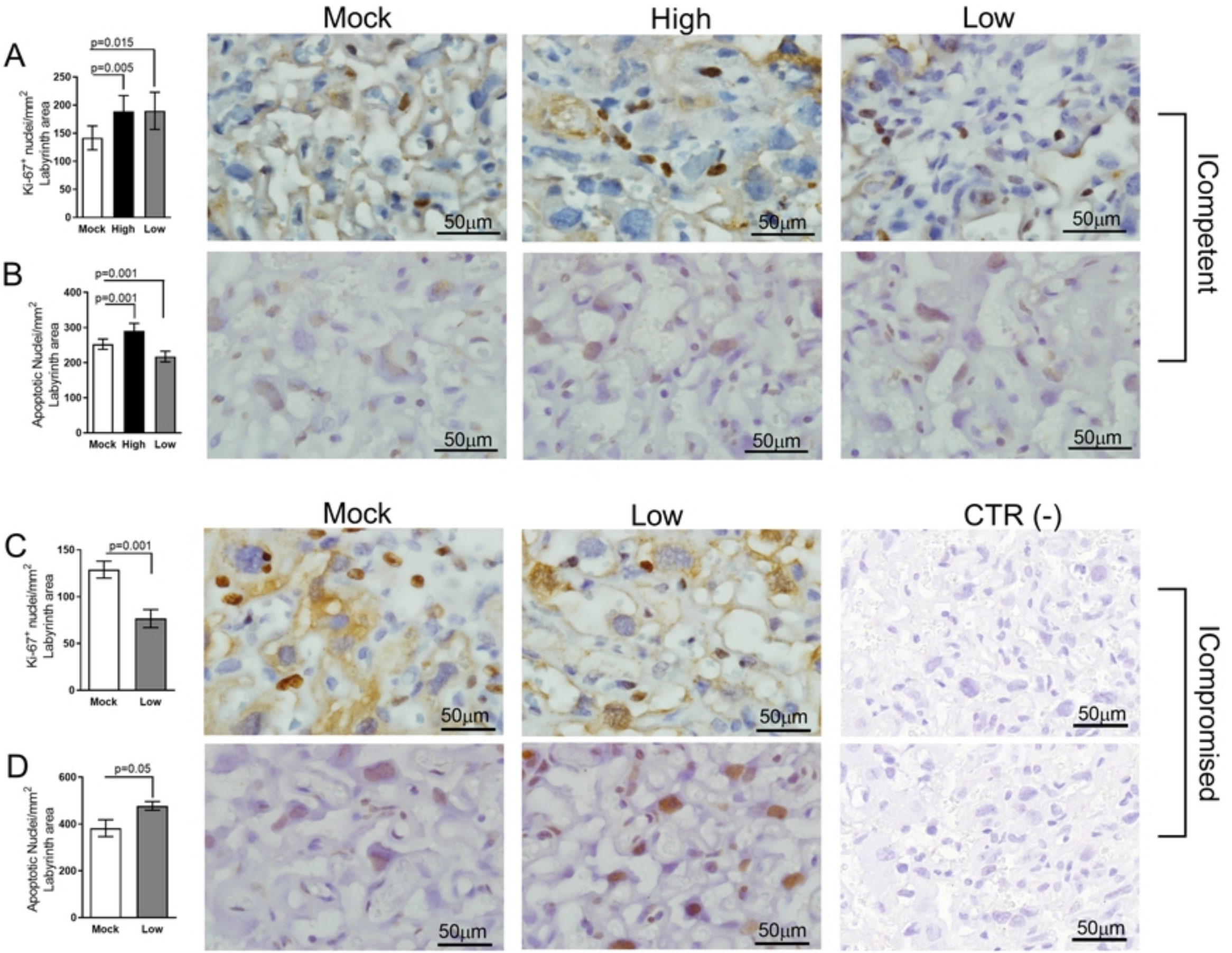
Mock
High
Low
A
p=0.015
p=0.005
Ki-67+ nuclei/mm2 Labyrinth area
250
200
150
100
50
0
Mock High Low
50µm
B
p=0.001
p=0.001
Apoptotic Nuclei/mm2 Labyrinth area
400
300
200
100
0
Mock High Low
ICompetent
Mock
Low
CTR (-)
C
p=0.001
Ki-67+ nuclei/mm2 Labyrinth area
150
100
50
0
Mock Low
D
p=0.05
Apoptotic Nuclei/mm2 Labyrinth area
600
400
200
0
Mock Low
ICompromised

Figure 4

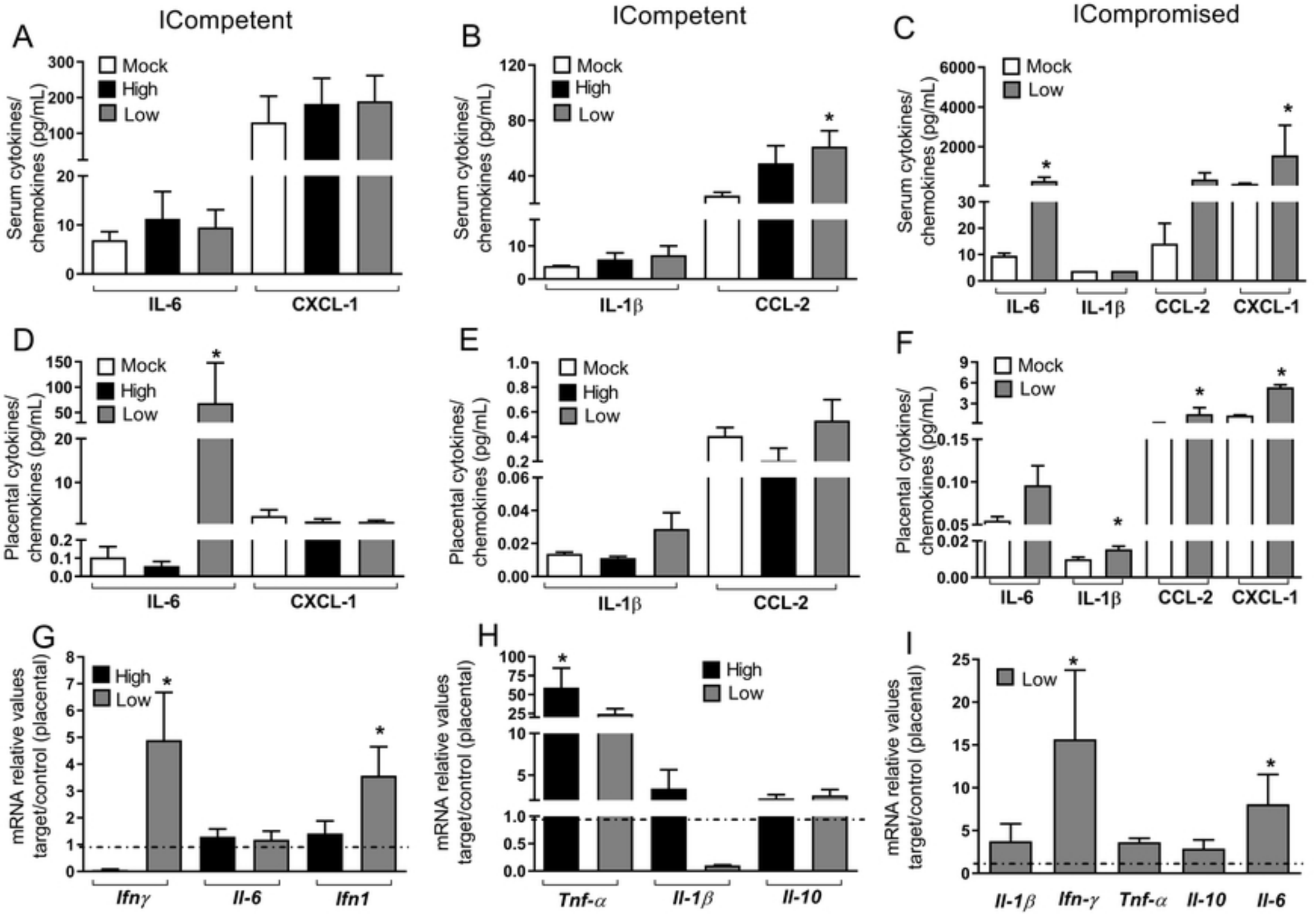
ICompetent
ICompetent
ICompromised
A
B
C
Mock
High
Low
Serum cytokines/ chemokines (pg/mL)
IL-6
CXCL-1
IL-1β
CCL-2
D
E
F
Placental cytokines/ chemokines (pg/mL)
G
H
I
mRNA relative values target/control (placental)
Ifnγ
Il-6
Ifn1
Tnf-α
Il-1β
Il-10
Ifn-γ

Figure 3

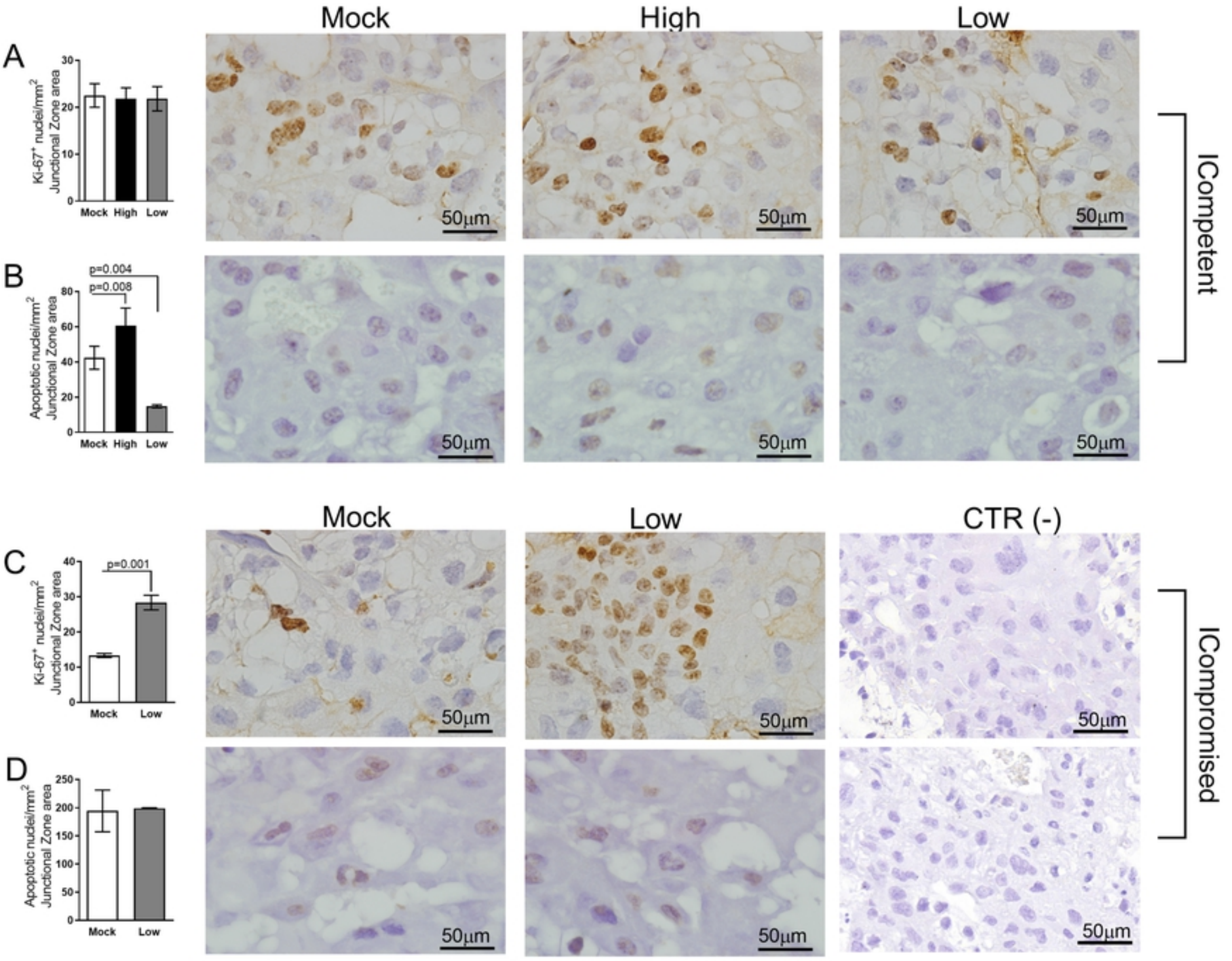
Mock
High
Low
A
Ki-67+ nuclei/mm2 Junctional Zone area
30
20
10
0
Mock High Low
50µm
50µm
50µm
B
p=0.004
p=0.008
Apoptotic nuclei/mm2 Junctional Zone area
80
60
40
20
0
Mock High Low
50µm
50µm
50µm
ICompetent
Mock
Low
CTR (-)
C
p=0.001
Ki-67+ nuclei/mm2 Junctional Zone area
40
30
20
10
0
Mock Low
50µm
50µm
50µm
D
Apoptotic nuclei/mm2 Junctional Zone area
250
200
150
100
50
0
Mock Low
50µm
50µm
50µm
ICompromised

Figure 5

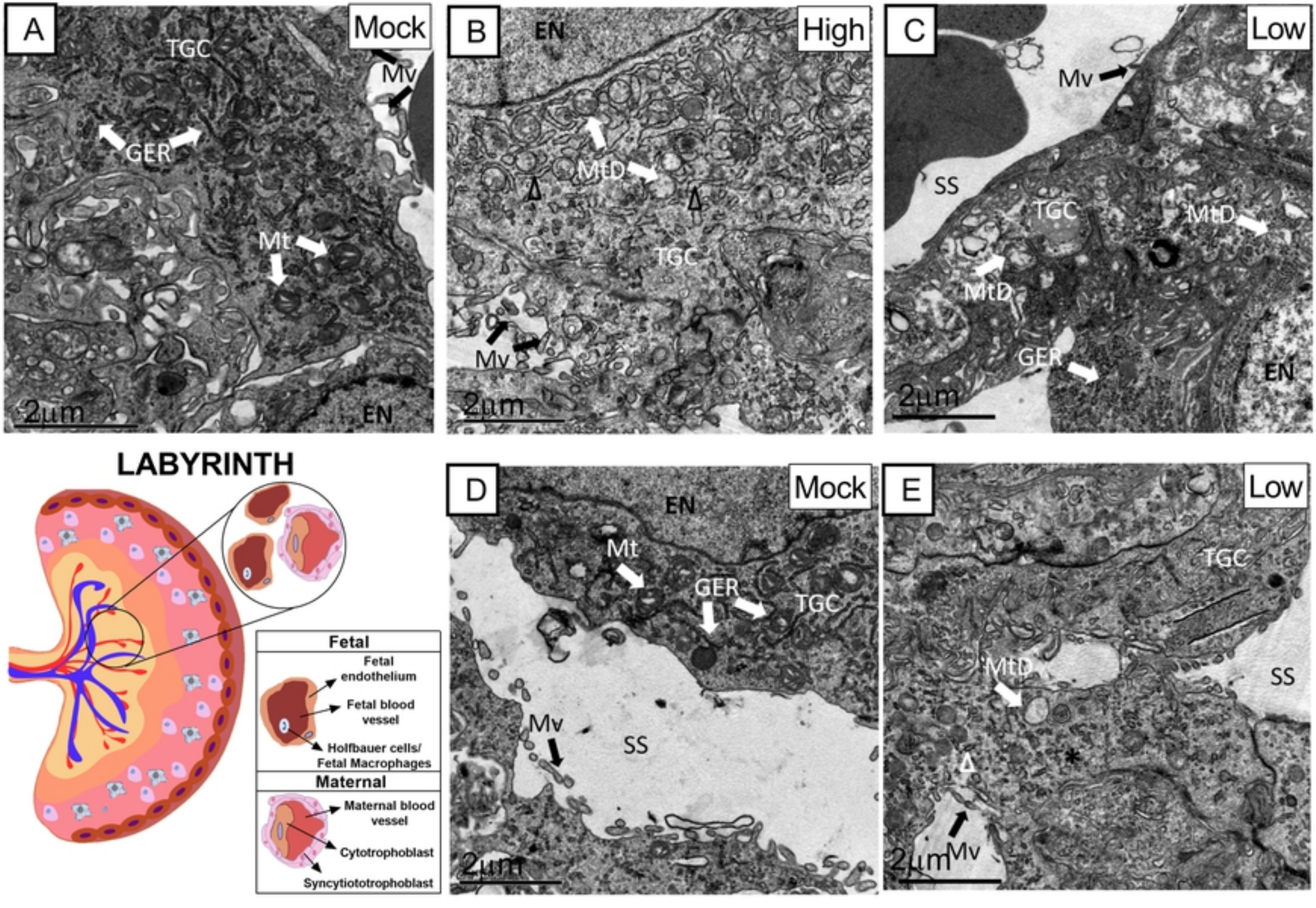
A
Mock
TGC
Mv
GER
Mt
EN
2µm
B
High
EN
MtD
TGC
Mv
2µm
C
Low
Mv
SS
TGC
MtD
MtD
GER
EN
2µm
LABYRINTH
Fetal
Fetal endothelium
Fetal blood vessel
Hofbauer cells/ Fetal Macrophages
Maternal
Maternal blood vessel
Cytotrophoblast
Syncytiotrophoblast
D
Mock
EN
Mt
GER
TGC
Mv
SS
2µm
E
Low
TGC
MtD
SS
Mv
2µm

Figure 6

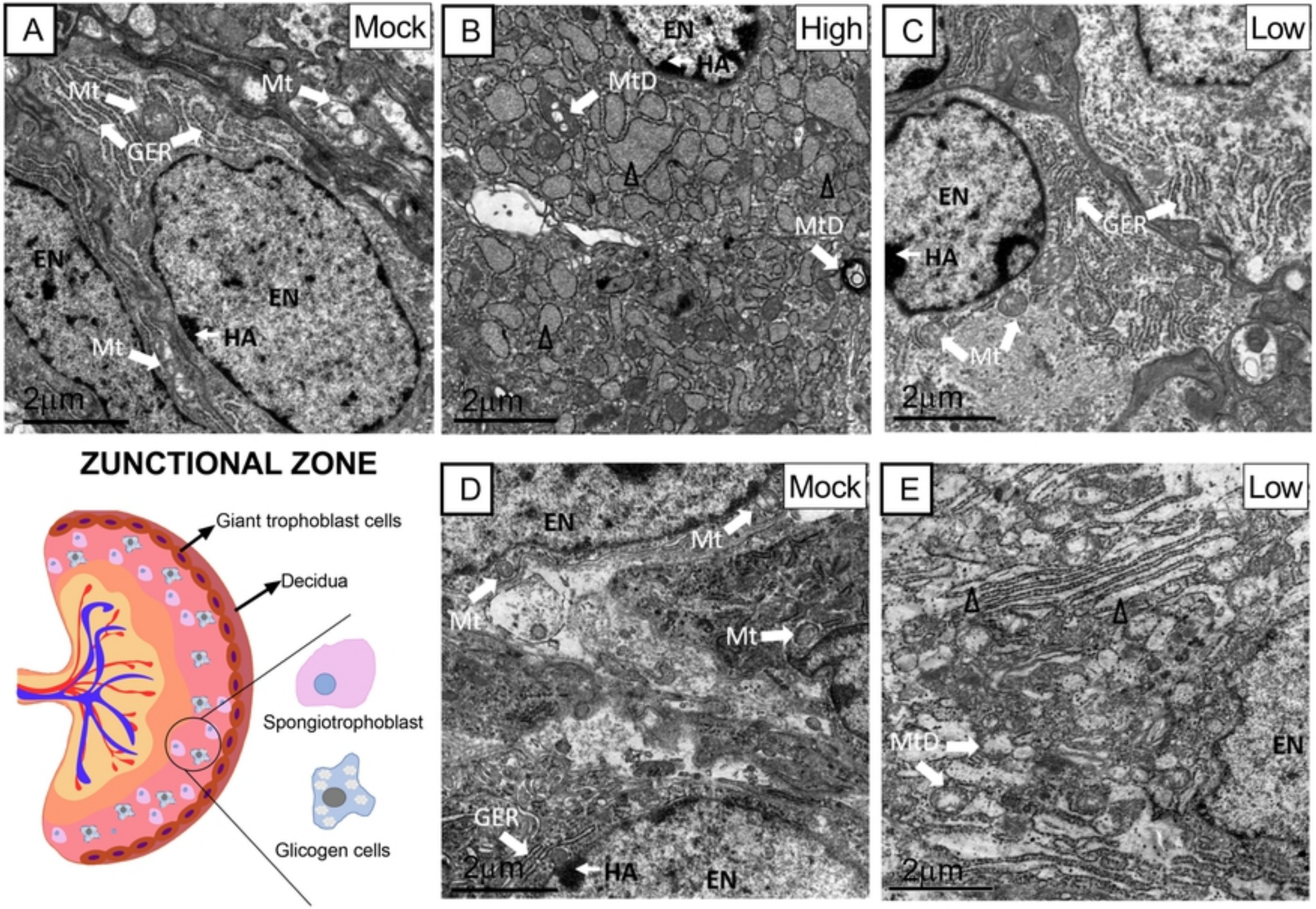
A
Mock
Mt
Mt
GER
EN
EN
HA
Mt
2µm
B
High
EN
HA
MtD
MtD
2µm
C
Low
EN
GER
HA
Mt
2µm
ZUNCTIONAL ZONE
Giant trophoblast cells
Decidua
Spongiotrophoblast
Glicogen cells
D
Mock
EN
Mt
Mt
Mt
GER
2µm
HA
EN
E
Low
MtD
EN
2µm

Figure 7

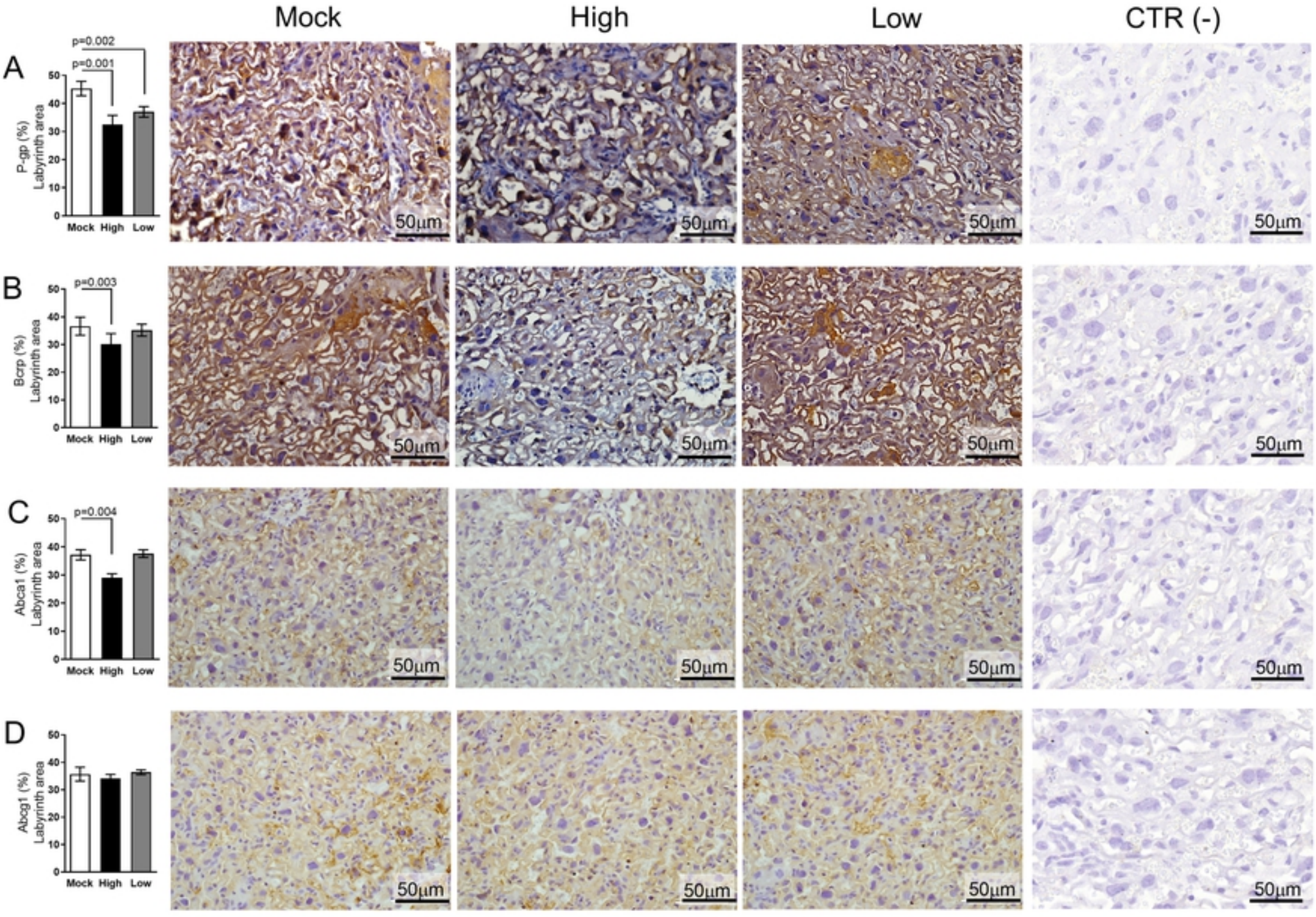
Mock
High
Low
CTR (-)
A
p=0.002
p=0.001
P-gp (%)
Labyrinth area
Mock High Low
B
p=0.003
Bcrp (%)
Labyrinth area
C
p=0.004
Abca1 (%)
Labyrinth area
D
Abcg1 (%)
Labyrinth area
50µm

Figure 8

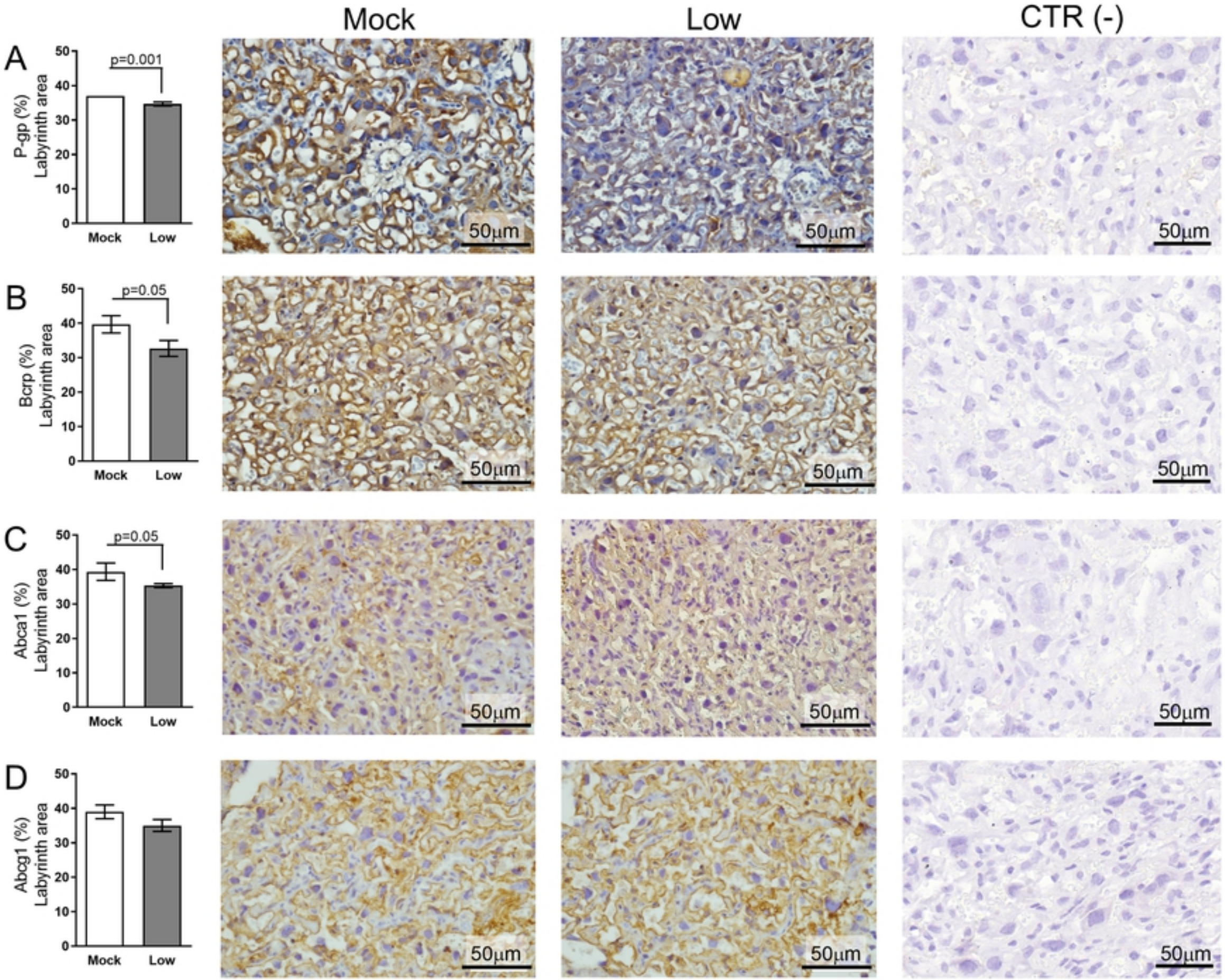
Mock
Low
CTR (-)
A
p=0.001
P-gp (%)
Labyrinth area
Mock
Low
50µm
B
p=0.05
Bcrp (%)
Labyrinth area
C
p=0.05
Abca1 (%)
Labyrinth area
D
Abcg1 (%)
Labyrinth area
0
10
20
30
40
50

Figure 9

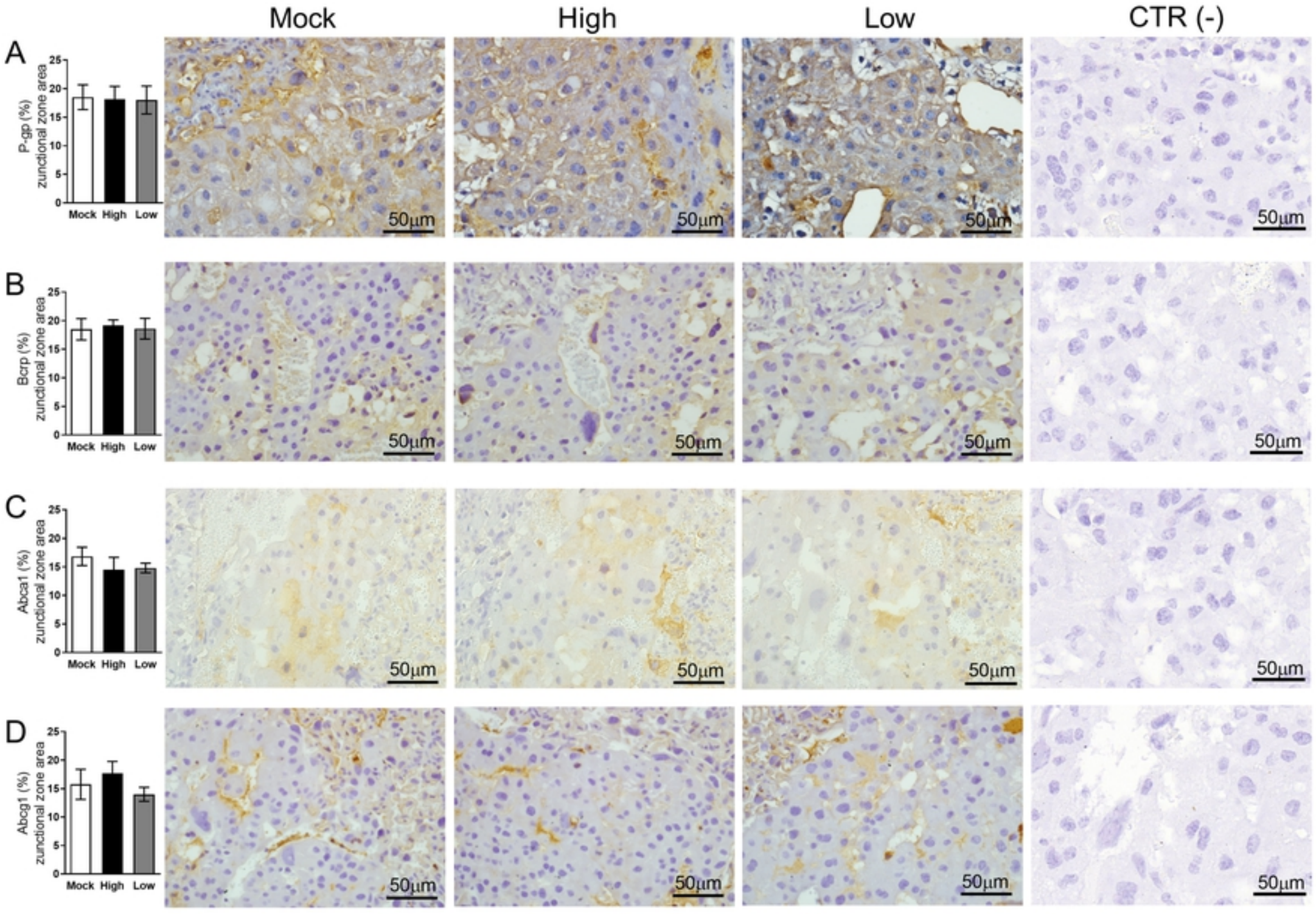
Mock
High
Low
CTR (-)
A
P-gp (%)
zunctional zone area
B
Bcrp (%)
zunctional zone area
C
Abca1 (%)
zunctional zone area
D
Abcg1 (%)
zunctional zone area
Mock High Low
50µm

Figure 10

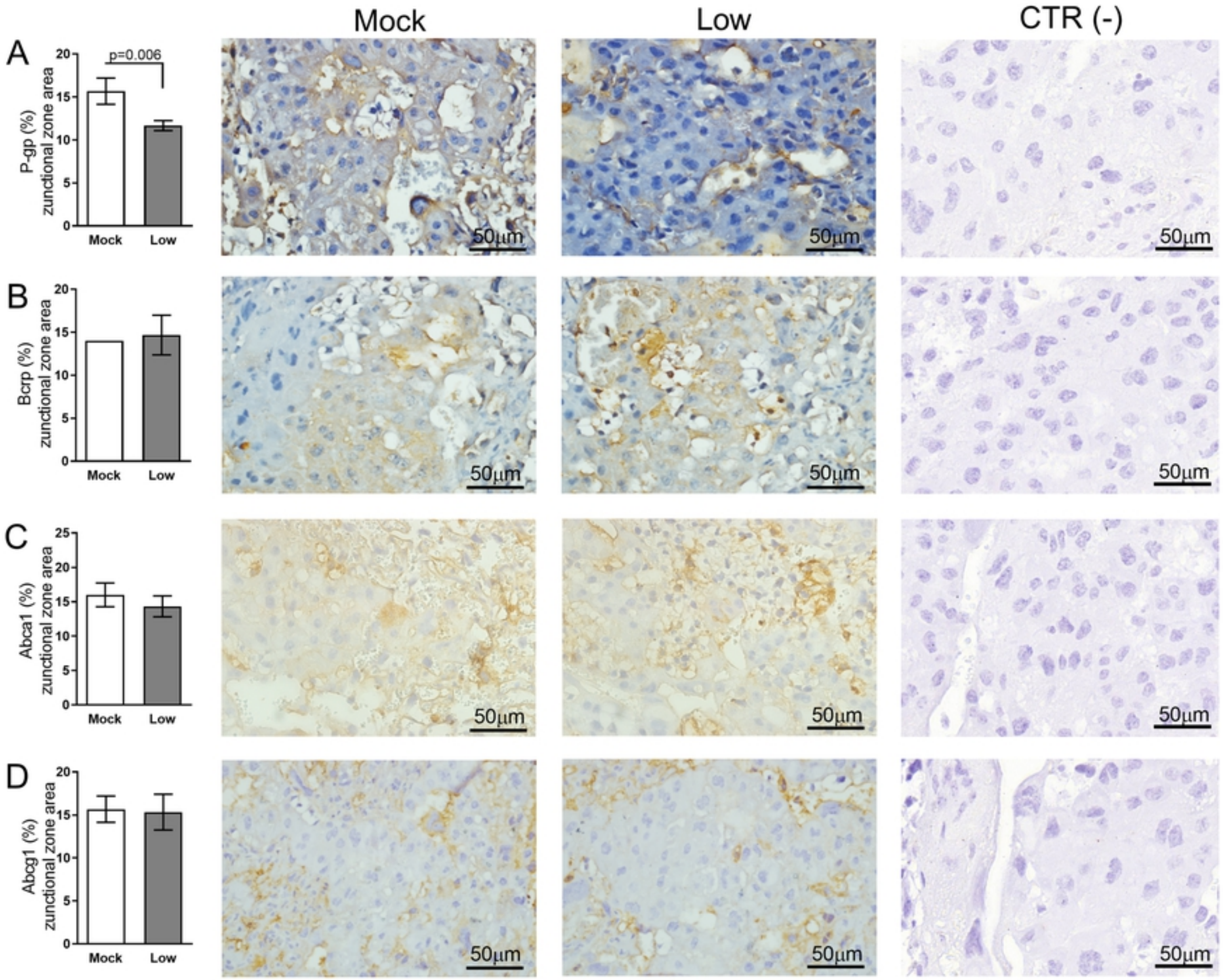
Mock
Low
CTR (-)
A
p=0.006
P-gp (%)
zunctional zone area
Mock
Low
B
Bcrp (%)
zunctional zone area
C
Abca1 (%)
zunctional zone area
D
Abcg1 (%)
zunctional zone area
50µm

Figure 11